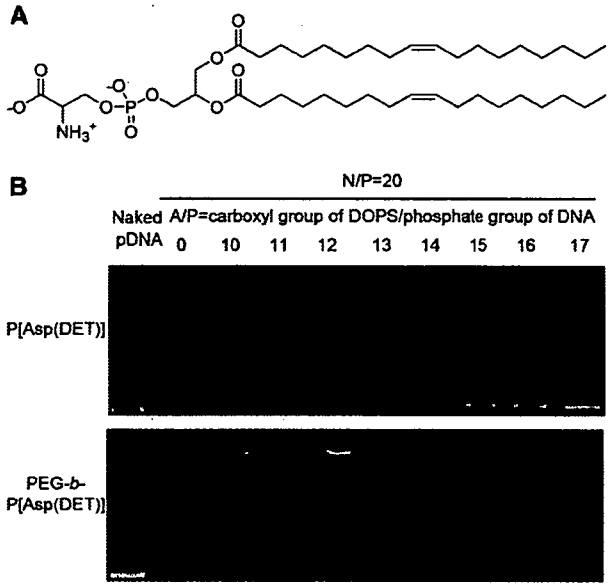

Fig. 7. Electrophoresis of P[Asp(DET)] polyplex and PEG-*b*-P[Asp(DET)] polyplex micelle. A) Chemical structure of anionic lipid (DOPS). B) Electrophoresis of P[Asp(DET)] polyplex and PEG-*b*-P[Asp(DET)] polyplex micelle solutions prepared at the *N/P* ratio of 20 after mixing with anionic lipid, DOPS at different *A/P* ratios.

cationic polymers and in some cases protected by biocompatible polymers to improve stability in biological media [9–12], prolonged evaluation of the gene expression might be necessary because it may take time for the decondensation and the release (the unpacking process) of pDNA from the polyplexes. Another important discrepancy between in vitro conventional monolayer cultures and in vivo tissues is the three-dimensional environments (e.g., cell–cell and cell–ECM interactions) for the cells. Thus, the three-dimensional features of in vivo tissues should be considered for in vitro evaluation of gene transfection. In this regard, three-dimensional multicellular spheroids (MCTS) might be a promising in vitro model for the evaluation of non-viral vectors worked under in vivo conditions.

In the transfection study using MCTS models, a long-term life span of MCTS might allow the prolonged evaluation of gene expression by non-viral vectors. Indeed, the spheroids transfected with the polyplexes showed the gene expression of fluorescent protein for over 10 days (Figs. 5 and 6). We also found that the small spheroids with diameters of ca 100 μm were more sensitive against the polyplex-induced cytotoxicity than monolayer cultured cells, while relatively large (ca 700 nm) MCTS did not show such high sensitivity to polyplex-induced toxicity (data not shown). It appears that the small spheroids may have a relatively weak structure due to their immature development of cell–cell and cell–ECM interactions. In contrast, the large spheroids have a heterogeneous structure consisting of outer layers of viable cells and a solid core of necrotic or hypoxic cells (Fig. 4C), resembling a monolayer cell culture where the cells adhere to the hard substrate. Such morphological differences between small and large spheroids may account for their different sensitivities against polyplex-induced cytotoxicity.

Among the evaluated polyplexes from the cationic homopolymers, P[Asp(DET)] polyplexes showed the most efficient transfection efficiency with the least cytotoxicity against monolayer cultured cells (Figs. 2 and 3). The efficient transfection by P[Asp (DET)] may be explained by their buffering capacity (Fig. 1A), which may facilitate the cytoplasmic delivery of the polyplexes through destabilization of the endosomal membrane by an increased ion osmotic pressure (proton sponge effect) [2]. However, P[Asp(DPT)] polyplexes at $N/P=10$ also showed an appreciably high transfection activity (Fig. 2A) regardless of the lack of proton buffering capacity (Fig. 1A), suggesting that the proton sponge effect may not fully explain the efficient gene transfection by P[Asp (DPT)] polyplex. Detailed mechanisms involved in the gene transfection process of P[Asp(DET)] and P[Asp(DPT)] polyplexes are under investigation in our laboratory and will be reported elsewhere in the near future. The cytotoxicity of P[Asp(DET)] polyplexes was remarkably low compared with other polyplexes from P[Asp(DPT)] or L/BPEI (Fig. 3). Also, the transfection study using MCTS models revealed that P[Asp(DET)] polyplexes at $N/P=10$ and 20 showed successful transfection with maintaining the MCTS structures, while the destruction of MCTS occurred by challenging L/BPEI and P[Asp(DPT)] polyplexes (Fig. 5B). The destruction of MCTS by the polyplexes (Fig. 5B) is in line with the cytotoxicity of the polyplexes against the monolayer cultured cells (Fig. 3), indicating the minimally cytotoxic nature of P[Asp(DET)] polyplexes. The unique molecular feature of a franking ethylene-diamine unit, including a specific *gauche*-conformation of the mono-protonated form preferential at the physiological state, may have a role in this appreciably high biocompatibility of P[Asp (DET)] polyplexes. This hypothesis remains to be clarified yet.

PEGylation of polycations apparently improved the biocompatibility of polyplexes, as indicated by the stability of the MCTS structure after transfection. The PEG-*b*-P[Asp(DPT)] polyplex micelles at $N/P=10$ did not cause the destruction of the MCTS (Fig. 5C), whereas the destruction occurred through the transfection with P[Asp(DPT)] polyplexes at the same *N/P* ratio (Fig. 5B). Likewise, the PEG-*b*-P[Asp(DET)] polyplex micelles at $N/P=40$ showed no MCTS destruction, while the destruction of MCTS was observed in the transfection with the P[Asp(DET)] polyplexes at the same *N/P* ratio. Note that such a difference in biocompatibility between PEG-*b*-P[Asp(DET)] polyplex micelles and P[Asp(DET)] polyplexes could not be detected by the cytotoxicity study using the monolayer cultured cells, but was detected using the MCTS models. This result suggests that MCTS models are more sensitive than monolayer cultured cells to polyplex-induced toxicity, allowing them to detect the improved biocompatibility of the polyplex system through the PEGylation of polycations. Besides its positive effect of improving the cytotoxicity of the polyplexes, PEGylation of the polyplex changed the time-dependent profiles of the transfected gene expression. As seen in Fig. 6C, the relative intensity of the transfected fluorescent protein (i.e., *Venus*) in MCTS, which is defined as the total intensity divided by the volume of spheroids, followed significantly different time courses between P[Asp(DET)] polyplexes and PEG-*b*-P[Asp(DET)] polyplex micelles: the latter with relatively high *N/P* ratios, such as 20 and 40, had peak relative intensities at 4 days after transfection, while the former exhibited a continuous decrease in the relative

intensities with time (Fig. 6C). These results suggest that the polyplex micelles from PEG-*b*-polycation copolymers may be capable of delaying gene expression compared with polyplexes from cationic homopolymers. This is consistent with our previous report that in vivo gene expression of polyplex micelles in the liver revealed a delayed onset, and was observed 5 days after intravenous injection [13]. We hypothesized that such delayed gene expression from the polyplex micelles might be due to their higher stability or their delayed unpacking of pDNA in intracellular compartments. This may be supported from the increased tolerability of PEG-*b*-P[Asp(DET)] polyplex micelles compared to P[Asp(DET)] polyplexes against the pDNA exchange reaction with an anionic lipid, DOPS (Fig. 7). It is also consistent with our previous report that PEG-*b*-poly(L-lysine) polyplex micelles showed higher stability than poly(L-lysine) polyplexes in the thermal melting study of DNA [8]. The decrease in the local permittivity of the polyplex core, surrounded by PEG palisades and/or a steric protection of the polyplex core by PEG palisades, may contribute to the stabilization of polyplex micelles against the exchange reaction with anionic components in intracellular environments. It is worth noting that the time-dependency of gene expression differs between polyplex systems, which was clearly investigated through the prolonged observation of transfected cells in the form of spheroids.

In conclusion, we used MCTS models to study the effects of chemical structures and PEGylation of cationic poly(*N*-substituted asparagine) polyplexes on gene transfection, particularly focusing on both polyplex toxicity and the duration of gene expression. Through this evaluation, the feasible properties, i.e., biocompatibility and prolonged gene expression, of PEG-*b*-P[Asp(DET)] micelles were clarified, facilitating their utility for in vivo gene transfection as recently demonstrated in a rabbit carotid artery model [15]. Also, this study underscores the usefulness of MCTS models in screening non-viral vectors in conditions mimicking in vivo environments.

Acknowledgement

We are grateful to Mr. S. Fukushima and Mr. S. Asano for polymer synthesis. This work was supported by the Core Research for Evolutional Science and Technology (CREST), Japan Science and Technology Agency (JST), and the Health and Labor Sciences Research Grants in Research on Advanced Medical Technology in Nanomedicine Area from the Ministry of Health, Labor and Welfare (MHLW), Japan.

Appendix A. Supplementary data

Supplementary data associated with this article can be found, in the online version, at doi:10.1016/j.jconrel.2007.05.012.

References

[1] G.Y. Wu, C.H. Wu, Receptor-mediated in vitro gene transformation by a soluble DNA carrier system, J. Biol. Chem. 262 (1987) 4429–4432.
[2] O. Boussif, F. Lezoualc'h, M.A. Zanta, M.D. Mergny, D. Scherman, B. Demeneix, J.P. Behr, A versatile vector for gene and oligonucleotide transfer into cells in culture and in vivo: Polyethyleneimine, Proc. Natl. Acad. Sci. U. S. A. 92 (1995) 7297–7301.
[3] D.W. Pack, A. Hoffman, S. Pun, P.S. Stayton, Design and development of polymers for gene delivery, Nat. Rev. Drug. Discov. 4 (2005) 581–593.
[4] A.V. Kabanov, I.V. Astafieva, I.V. Maksimova, E.M. Lukanidin, G.P. Georgiev, V.A. Kabanov, Efficient transformation of mammalian cells using DNA interpolyelectrolyte complexes with carbon chain polycations, Bioconjug. Chem. 4 (1993) 448–454.
[5] M. Harada-Shiba, K. Yamauchi, A. Harada, I. Takamisawa, K. Shimokado, K. Kataoka, Polyion complex micelles as vectors in gene therapy — pharmacokinetics and in vivo gene transfer, Gene Ther. 9 (2002) 407–414.
[6] M. Ogris, E. Wagner, Targeting tumors with non-viral gene delivery systems, Drug Discov. Today 7 (2002) 479–485.
[7] K. Kataoka, G.S. Kwon, M. Yokoyama, T. Okano, Y. Sakurai, Block copolymer micelles as vehicles for drug delivery, J. Control. Release 24 (1993) 119–132.
[8] S. Katayose, K. Kataoka, Water-soluble polyion complex associates of DNA and poly(ethylene glycol)-poly(l-lysine) block copolymer, Bioconjug. Chem. 8 (1997) 702–707.
[9] M. Ogris, S. Brunner, S. Schüller, S. Kircheis, E. Wagner, PEGylated DNA/transferrin-PEI complexes: reduced interaction with blood components, extended circulation in blood and potential for systemic gene delivery, Gene Ther. 6 (1999) 595–605.
[10] T. Merdan, K. Kunath, H. Petersen, U. Bakowsky, K.H. Voigt, J. Kopecek, T. Kissel, PEGylation of poly(ethylene imine) affects stability of complexes with plasmid DNA under in vivo conditions in a dose-dependent manner after intravenous injection in to mice, Bioconjug. Chem. 16 (2005) 785–792.
[11] K. Itaka, A. Harada, K. Nakamura, H. Kawaguchi, K. Kataoka, Evaluation by fluorescence resonance energy transfer of the stability of nonviral gene delivery vectors under physiological conditions, Biomacromolecules 3 (2002) 841–845.
[12] K. Itaka, K. Yamauchi, A. Harada, K. Nakamura, H. Kawaguchi, K. Kataoka, Polyion complex micelles from plasmid DNA and poly(ethylene glycol)-poly (l-lysine) block copolymers as serum-tolerable polyplex system: physicochemical properties of micelles relevant to gene transfection efficiency, Biomaterials 24 (2003) 4495–4506.
[13] K. Miyata, Y. Kakizawa, N. Nishiyama, Y. Yamasaki, T. Watanabe, M. Kohara, K. Kataoka, Freeze-dried formulations for in vivo gene delivery of PEGylated polyplex micelles with disulfide crosslinked cores to the liver, J. Control. Release 109 (2005) 15–23.
[14] N. Kanayama, S. Fukushima, N. Nishiyama, K. Itaka, W.D. Jang, K. Miyata, Y. Yamasaki, U.I. Chung, K. Kataoka, A PEG-based biocompatible block catiomer with high buffering capacity for the construction of polyplex micelles showing efficient gene transfer toward primary cells, Chem. Med. Chem. 1 (2006) 439–444.
[15] D. Akagi, M. Oba, H. Koyama, N. Nishiyama, S. Fukushima, T. Miyata, H. Nagawa, K. Kataoka, Biocompatible micellar nanovectors achieve efficient gene transfer to vascular lesions without cytotoxicity and thrombus formation. Gene Therapy, in press.
[16] R.M. Sutherland, Cell and environment interactions in tumor microregions: the multicell spheroid model, Science 240 (1988) 177–184.
[17] H.R. Mellor, L.A. Davies, H. Caspar, C.R. Pringle, S.C. Hyde, D.R. Gill, R. Callaghan, Optimising non-viral gene delivery in a tumour spheroid model, J. Gene Med. 8 (2006) 1160–1170.
[18] H. Niwa, K. Yamamura, J. Miyazaki, Efficient selection for high-expression transfectants with a novel eukaryotic vector, Gene 108 (1991) 193–199.
[19] T. Nagai, K. Ibata, E.S. Park, M. Kubota, K. Mikoshiba, A. Miyawaki, A variant of yellow fluorescent protein with fast and efficient mutation for cell-biological application, Nat. Biotechnol. 20 (2002) 87–90.
[20] G.P. Tang, J.M. Zeng, S.J. Gao, Y.X. Ma, L. Shi, Y. Li, H.P. Too, S. Wang, Polyethylene glycol modified polyethylenimine for improved CNS gene transfer, Biomaterials 24 (2003) 2351–2362.
[21] M. Haji-Karim, J. Carlsson, Proliferation and viability in cellular spheroids of human origin, Cancer Res. 38 (1978) 1457–1464.
[22] L.A. Kunz-Schughart, Multicellular tumor spheroids; intermediates between monolayer culture and in vivo tumor, Cell Biol. Int. 23 (1999) 157–161.

In Vivo Antitumor Activity of the Folate-Conjugated pH-Sensitive Polymeric Micelle Selectively Releasing Adriamycin in the Intracellular Acidic Compartments

Younsoo Bae,[†,‡] Nobuhiro Nishiyama,[†,‡] and Kazunori Kataoka*[,†,‡,§]

Center for Disease Biology and Integrative Medicine, Graduate School of Medicine, The University of Tokyo, 7-3-1 Hongo, Bunkyo-ku, Tokyo 113-0033, Japan, and Center for NanoBio Integration and Department of Materials Engineering, The University of Tokyo, 7-3-1 Hongo, Bunkyo-ku, Tokyo 113-8656, Japan. Received December 26, 2006; Revised Manuscript Received March 2, 2007

Cancer treatment efficacy and safety of the environmentally sensitive polymeric micelle drug carriers were significantly increased by optimizing the number of ligands on their surface. These micelles were designed to target the cancerous tumors through the interaction between folate and its receptors that overexpress on the cancer cell membrane while achieving pH-controlled drug release in the intracellular acidic compartments such as endosomes and lysosomes. In order to elucidate the effects of folate on cytotoxicity, biodistribution, anticancer activity, and pharmacological properties, folate concentration on the surface of the micelles was controlled by precise synthesis of two different amphiphilic block copolymers that self-assemble into spherical micelles, folate–poly(ethylene glycol)–poly(aspartate-hydrazone-adriamycin) with γ-carboxylic acid activated folate and methoxy-poly(ethylene glycol)–poly(aspartate-hydrazone-adriamycin) without folate. It is of significance that, although folate conjugation induced an extremely small change in tumor accumulation of the micelles, folate-conjugated micelles showed lower in vivo toxicity and higher antitumor activity over a broad range of the dosage from 7.50 to 26.21 mg/kg, which was 5-fold broader than free drugs.

INTRODUCTION

Precise control of the amount and uniform distribution of ligands on nanoparticles is one of the most challenging assignments in the design of polymeric drug carriers for successful active drug targeting (*1*–*3*). Indeed, a large number of studies have shown that active drug targeting is promising for effective cancer treatment (*4*–*7*). However, the questions about how many ligands are necessary for achieving efficient active drug targeting of the polymeric drug carriers are still controversial and remain to be elucidated further. In particular, when such drug carriers are tailored to deliver anticancer drugs to cancer cells systemically, it is of significant importance to confirm whether the ligand conjugation maintains their pharmacokinetic properties without decreasing antitumor activity. It is because anticancer drugs are normally highly toxic, inducing serious side effects, and although ligands can increase the interaction between the drug carriers and targeted cells in the body, they might also induce an increase in the cellular interaction with nontargeted cells, that we are not willing to deliver drugs. In order to answer these questions, we have to prepare first a drug carrier with optimal amounts of ligands, whose chemical and biological properties are fairly well established and then ascertain whether ligand installation induces any change in its biological properties.

The rationales for tumor-specific drug delivery with polymers have been reported during the past decades and are based on the characteristics of tumor tissues such as disordered and leaky vasculatures, a thick extracellular matrix, and other microenvironmental peculiarities including the hypoxic environment, expression of cancer-specific receptors, and excessive secretion of cytokines (*8*–*9*). One of the widely accepted methodologies for polymeric drug delivery is to target leaky tumor vessels and the poorly developed lymphatic drainage in the tumor tissues so that polymers and their drug conjugates can pass the tumor blood vessel wall and then accumulate in tumor tissue for a prolonged time. This methodology is explained as the enhanced permeability and retention (EPR) effect, providing the most probable theory for passive drug targeting (*10*). Nevertheless, recent studies have revealed that tumor-targeting drug delivery cannot be completely achieved only by the EPR effect because polymeric drug carriers often encounter difficulties in accessing cancer cells in the deeper place of the tumor tissues or in interacting with the targeted cells after accumulation (*11, 12*). Polymeric drug carriers are normally required to have biocompatibility and high molecular weight to prevent protein adsorption that induces recognition by the body defense system and to increase the tumor accumulation via the EPR effect, respectively. However, these efforts frequently result in low cellular uptake of polymeric drug carriers after extravasation, reducing the actual drug concentration within the tumor due to the stagnation around the tumor tissue. As a result, we should inject polymeric drug carriers with a higher amount compared to free drugs to deliver a sufficient amount of drugs to the tumor. This is also the reason the current polymeric drug delivery systems urgently need to improve their targeting efficiency. From these aspects, active targeting has been believed to clear the problems by facilitating polymeric drug delivery systems (*13*). Active targeting can be achieved by installing ligands to the polymers or polymer assemblies so that they can interact with receptors that express on the targeted sites such as cancer cell membranes. Nevertheless, it is obvious that active targeting

* To whom correspondence should be addressed: Kazunori Kataoka, Ph.D. Professor, Department of Materials Engineering, Graduate School of Engineering, The University of Tokyo, 7-3-1 Hongo, Bunkyo-ku, Tokyo 113-8656, Japan. Phone +81-3-5841-7138, Fax +81-3-5841-7139, E-mail: kataoka@bmw.t.u-tokyo.ac.jp.

† Graduate School of Medicine.

‡ Center for NanoBio Integration.

§ Department of Materials Engineering.

10.1021/bc060401p CCC: $37.00
Published on Web 05/09/2007

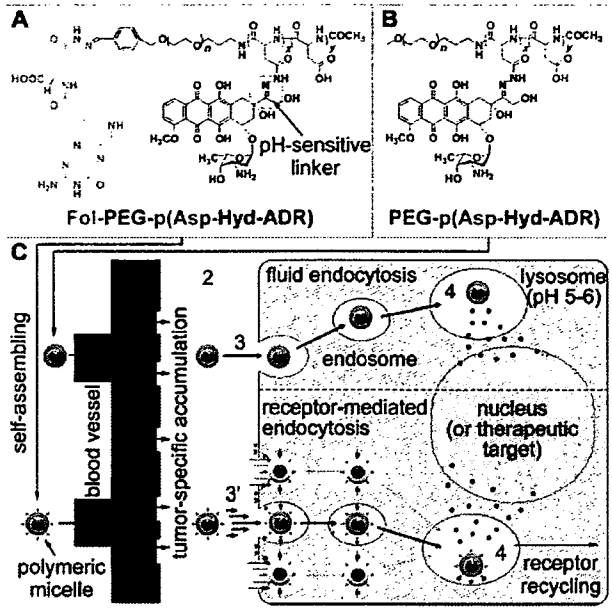

Figure 1. Design of polymeric micelles and the rationale for active drug delivery. Chemical structures of folate–poly(ethylene glycol)–poly(aspartate-hydrazone-adriamycin) and methoxy-poly(ethylene glycol)–poly(aspartate-hydrazone-adriamycin) block copolymers (A and B). As shown in panel C, these polymers can self-assemble into the polymeric micelles that can effectively achieve systemic drug delivery and tumor-specific accumulation (1 and 2). The micelles are then uptaken by the cancer cells via fluid endocytosis (3) or receptor-mediated endocytosis (3′) depending on surface design for accelerating endocytosis (e.g., folate conjugation). Anticancer drugs, adriamycin (ADR), that are conjugated through a pH-sensitive hydrazone bond can be released from the micelles in the acidic intracellular compartments such as endosomes or lysosomes where pH ranges from 5 to 6 (4).

cannot be achieved until passive targeting of drug carriers is successfully accomplished.

Amphiphilic block copolymers are useful tools for the preparation of supramolecular assemblies. By precisely controlling their molecular weight and the hydrophilic/hydrophobic balance, we can prepare spherical supramolecular nanoassemblies, also known as "the polymeric micelles", with a hydrophilic shell that envelopes a hydrophobic core (*14*). The polymeric micelle is considered to be one of the most successful polymeric drug carrier formulations, because it is characterized by high drug loading contents, prolonged blood circulation, and selective tumor accumulation (*15*). Most notably, their chemical, biological, and pharmacological properties have been widely studied, and thus we can easily investigate the effect of active targeting (*16, 17*). In this study, poly(ethylene glycol)–poly(β-benzyl-L-aspartate) block copolymers (PEG–PBLA) were synthesized for the basic platform for the preparation of the polymeric micelles, and these micelles were further functionalized to conjugate anticancer drugs and ligands. Figure 1 shows the chemical structures of the block copolymers used in this study. Anticancer drugs, adriamycin (ADR), were conjugated to the side chains of the core-forming poly(aspartic acid) block through a hydrazone linkage, which can be selectively cleaved under the acidic conditions with pH ranging from 5 to 6, corresponding to the intracellular vesicles such as the endosomes and lysosomes (*18*). In our previous studies, we have reported that this intracellular pH-sensitive polymeric micelle showed remarkably low toxicity and high in vivo efficacy (*19*). It was also confirmed that the pH-sensitive micelles can release drugs selectively by responding to a decrease in intracellular pH of the cell, and therefore, drug leakage from the micelles decreases during the blood circulation and tumor-specific drug delivery efficiency increases. In the meantime, folate was conjugated at the end of the shell-forming poly(ethylene glycol) (PEG) block for active targeting. Folate, an anionic form of folic acid, is a vitamin B9 that helps the production and maintenance of new cells. Originally, folate was necessary for the restoration of the DNA damage that may induce cancer. However, interestingly, cancer cells overexpress folate-binding proteins (FBPs) on their cell membranes (*20, 21*). This is probably due to the DNA replication that is supported by folate, which is also a prerequisite for the cancer growth. More interestingly, cancer cells are believed to reduce chemotherapeutical response by regulating intracellular folate concentration (*22*). Therefore, we can actively guide polymeric drug carriers to cancer cells in the body by folate conjugation (*23*). It must be noticed that FBP binding activity of folate drastically changes depending on its activated state, which is distinguished by an inactive α- and active γ-carboxyl activated form (*24*). Herein, we conjugated folate to PEG at its γ-carboxyl position to maintain its activity by precision synthesis as reported elsewhere (*25–27*).

The objectives of this research are to ascertain whether folate conjugation can enhance antitumor efficacy of the pH-sensitive micelles without deteriorating the characteristics of the micelles as a long-circulating drug carrier with high tumor accumulation, and to determine how much folate concentration is optimum for achieving effective passive and active drug targeting simultaneously. Such information would be beneficial to the future design and preparation of ligand-installed multifunctional polymeric drug carriers for cancer treatment.

EXPERIMENTAL PROCEDURES

Materials and Devices. Acetic anhydride (AA), chloroform ($CHCl_3$), *N,N*-dimethyl formamide (DMF), dimethyl sulfoxide (DMSO), hexane, methanol (MeOH), methanesulfonyl chloride (CH_3SO_2Cl), triethylamine (TEA), trifluoroacetic acid (TFA), trifluoroacetic anhydride (TFAA), and tetrahydrofuran (THF) were purchased from Wako Pure Chemical Industries, Japan. DMF, hexane, and THF were distilled twice following standard procedures. Carbazic acid *tert*-butyl ester (CAt-BE) and potassium carbonate (K_2CO_3) were purchased from Tokyo Kasei Organic Chemicals, Japan. These chemicals were used without further purification. Daunorubicin (DAU), folic acid (Fol), 4-(diethoxymethyl)benzaldehyde, and sodium borohydride ($NaBH_4$) were purchased from Sigma Chemical, U.S.A. Ethylene oxide (EO) was from Sumitomo Seika Chemicals, Japan, and dried over calcium hydride followed by distillation. β-Benzyl-L-aspartate (BLA) was from Sigma, and α-methoxy-ω-amino-poly(ethylene glycol) (MeO-PEG-NH_2) was from Nippon Oil and Fats, Japan. PEG was purified using an ion-exchange gel column (CM-Sephadex C-50, Amersham Pharmacia Biotech, U.S.A.) prior to the synthesis of the block copolymers. Adriamycin hydrochloride (ADR) was kindly provided by Nippon Kayaku, Japan, and its purity was checked by reversed-phase liquid chromatograpy (RPLC). Sephadex LH-20 gel was from Amersham Pharmacia Biotech, Sweden. Gel permeation chromatography (GPC) analysis was carried out using a TOSOH HLC-8220 equipped with TSK-GEL columns (G4000PWXL and G3000PWXL). Internal refractive index (RI) and ultraviolet–visible absorption (UV) detectors were used. DMF containing 10 mM of LiCl was used as an eluant at a flow rate of 0.8 mL/min at 40 °C. ^1H NMR spectra were measured with a JEOL EX300 spectrometer (JEOL, Japan). Flow cytometric analysis was performed with EPICS XL Flow Cytometry Systems (Beckman Coulter, U.S.A.). The multimode reader Mithras LB 940 (Berthold Technologies, U.S.A.) was used for in vitro cytotoxicity evaluation using a CellTiter-Glo luminescent cell viability assay kit (Promega, U.S.A.).

Cell Lines and Animals. A human pharyngeal cancer cell line KB was purchased from Health Science Research Resources Bank, Japan. Cells were cultured in Dulbecco's Modified Eagle cell culture Medium (DMEM, Sigma, U.S.A.) containing 10% FBS under a humidified atmosphere with 5% CO_2 at 37 °C. CD-1 nude mice (female, 6-week-old) were purchased from Charles River, Japan. The animals were cared for and all experiments were performed in compliance with the Guide for the Care and Use of Laboratory Animals as adopted and promulgated by the National Institutes of Health. The number of independent experiments is stated as *n*, and the experimental data are expressed as mean and mean ± SEM for relative and absolute values, respectively.

Synthesis of Self-Assembling Amphiphilic Block Copolymers. In this study, we synthesized two different types of self-assembling amphiphilic block copolymers for the preparation of the micelles, folate−poly(ethylene glycol)−poly(aspartate-hydrazone-adriamycin) [Fol−PEG−p(Asp-Hyd-ADR)] and methoxy-poly(ethylene glycol)−poly(aspartate-hydrazone-adriamycin) [PEG−p(Asp-Hyd-ADR)]. Synthesis methods for these block copolymers were previously reported elsewhere (*25*). Briefly, Fol−PEG−p(Asp-Hyd-ADR) was synthesized via seven steps as follows.

a. Synthesis of Heterobifunctional α-4-(Diethoxymethyl)-benzylacetal-ω-amine-poly(ethylene glycol) (aceBz-PEG-NH_2). 4-(Diethoxymethyl)benzaldehyde (5 g) was reduced with $NaBH_4$ (1 g) in dry ethanol (100 mL). Obtained 4-(diethoxymethyl)-benzylalcohol (0.19 g) was then mixed with potassium naphthalene (115 mg) in dry THF (30 mL) to prepare potassium 4-(diethoxymethyl)benzylalkoxide, followed by the addition of distilled EO (11.9 g) for anionic polymerization to obtain aceBz-PEG-OH. After 2 days of reaction at 25 °C, CH_3SO_2Cl (0.62 g) and TEA (0.82 g) were added to aceBz-PEG-OH in 25 mL of THF to prepare an intermediate product aceBz-PEG-OSO_2CH_3, which was then mixed with ammonia solution (25%) to produce aceBz-PEG-NH_2.

b. Selective Functionalization of Folic Acid at its γ-Position of the Glutamate Residue with Hydrazide (Fol-hyd). An excess amount of TFAA (3 mL) was added dropwisely to folic acid (2 g) in THF (20 mL) to prepare N_{10}-(trifluoroacetyl)pyrofolic acid. This pyrofolic acid (500 mg) was reacted with CAt-BE (1.6 g) in 20 mL of dry DMF at 40 °C overnight. Prepared folate-hydrazide-BOC was treated with TFA to obtain Fol−Hyd.

c. Preparation of β-benzyl-L-aspartate N-Carboxy Anhydride (BLA−NCA). 5.77 g of triphosgene was added to 10 g of β-benzyl-L-aspartate in 150 mL of dry THF at 40 °C, and the reaction was allowed to proceed until the solution became clear. Prepared β-benzyl-L-aspartate *N*-carboxy anhydride (BLA−NCA) was purified by recrystallization from hexane.

d. Ring-Opening Polymerization of BLA−NCA by Using aceBz-PEG-NH_2 as a Macroinitiator to Obtain 4-(Diethoxymethyl)benzyl Acetal−poly(ethylene glycol)−poly(β-benzyl-L-aspartate) (aceBz−PEG−PBLA). 6 g of aceBz−PEG−NH_2 with molecular weight of 12 000 and 5 g of BLA−NCA were dissolved in 30 mL and 10 mL of DMSO, respectively. NCA solution was added to PEG solution at 40 °C, and the reaction was allowed to proceed for 2 days.

e. ω-Amino Group Protection for aceBz−PEG−PBLA Block Copolymers, Followed by α-Acetal Group Deprotection and Subsequent Conjugation of Fol−hyd at the End of the PEG Chain (Fol−PEG−PBLA). The ω-amino group of aceBz−PEG−PBLA was protected by AA to prevent dimerization between aldehyde−benzyl−poly(ethylene glycol)−poly(β-benzyl-L-aspartate) (CHO−Bz−PEG−PBLA) block copolymers, which can be prepared by deprotecting acetal groups of aceBz−PEG−PBLA with 0.1 N HCl aqueous solution. End-group protected CHO−Bz−PEG−PBLA (250 mg) was then mixed with Fol−Hyd (50 mg) in dry DMF to prepare Fol−PEG−PBLA.

Table 1. Polymer Compositions

compound	composition[a]	polydispersity index[d] (Mw/Mn)	drug loading content (wt %)
PEG-PBLA	12−42[b]	1.12	
Fol-PEG-PBLA	12−40[b]	1.14	
PEG-p(Asp-Hyd-ADR)	12−42−33−15[c]		33.84
Fol-PEG-p(Asp-Hyd-ADR)	12−40−34−14[c]		34.32

[a] The compositions of the block copolymers are abbreviated *X*−*Y* and *X*−*Y*−*Z*−*A*. The letter *X* stands for molecular weight × 10^{-3} of poly(ethylene glycol), while *Y*, *Z*, and *A* denote the numbers of aspartic acid, hydrazide, and adriamycin (ADR), respectively. [b] The values were calculated from the peak area ratio determined by ^{1}H NMR between poly(ethylene glycol) and benzyl groups of the PBLA block. [c] The numbers of hydrazide groups and ADR were determined by ^{1}H NMR and reversed-phase liquid chromatography (RPLC), respectively. [d] Polydispersity was measured for PEG−PBLA and Fol−PEG−PBLA to ensure the purity of starting materials.

f. Substitution Benzyl Esters at the Side Chain of Fol−PEG−PBLA with Drug-Binding Hydrazide Groups to Prepare Fol−PEG−p(Asp-Hyd). 500 mg of Fol−PEG−PBLA was dissolved in 10 mL of dry DMF, and anhydrous hydrazine (0.62 mg) was added to the solution. The reaction was allowed to proceed at 40 °C for 2 h, followed by deprotection of remained benzyl groups with 0.1 N NaOH aqueous solution at 25 °C. Polymers were dialyzed against 0.25% ammonia solution and collected by freeze-drying.

g. Conjugation of ADR at Its 13-C Carbonyl with the Hydrazide Groups of Fol−PEG−p(Asp-Hyd) through a pH-Sensitive Schiff Base Linkage. Fol−PEG−p(Asp-Hyd) (100 mg) in 50 mL of DMSO was mixed with an excess amount of ADR-HCl (100 mg) with respect to drug-binding hydrazide residues. The mixed solution was stirred at room temperature for 3 days. After precipitation from ether, Fol−PEG−p(Asp-Hyd-ADR) was redissolved in 10 mL of DMF and purified by gel filtration using a Sephadex LH-20 column. In the case of PEG−p(Asp-Hyd-ADR), MeO-PEG-NH_2 was used as a macroinitiator for BLA−NCA polymerization at step (d) instead of aceBz−PEG-NH_2, following the procedures from steps (e) to (g).

Preparation of the Folate-Conjugated pH-Sensitive Polymeric Micelles. The folate-conjugated pH-sensitive polymeric micelles were prepared from Fol−PEG−p(Asp-Hyd-ADR) alone or in combination with PEG−p(Asp-Hyd-ADR) block copolymers in various molar ratios to change folate contents (0%, 1%, 2%, 5%, 10%, 25%, 50%, and 100%). We distinguish the micelles from Fol−PEG-p(Asp-Hyd-ADR) and PEG−p(Asp-Hyd-ADR) by the notations of FMA and MA, which denote folate-conjugated micellar adriamycin and micellar adriamycin, respectively. For the preparation of FMA and MA, 250 mg of each Fol−PEG−p(Asp-Hyd-ADR) and PEG−p(Asp-Hyd-ADR) were dissolved in 5 mL of DMSO. Polymer solutions were then added dropwise into 95 mL of Tris−HCl buffer solution (10 mM, pH 7.4), sonicated at 25 °C for 10 min, and diluted further with 900 mL of Tris−HCl buffer. The polymer solutions were concentrated by Amicon Ultra-15 Centrifugal Filter Units (Millipore, U.S.A.) with molecular weight cutoff (MWCO) 30 000 kDa. 12 mL of the solutions in each swinging bucket rotor were spun at 1500 *g* at 25 °C for 15 min. During repetitive centrifugation, additional Tris−HCl buffer was added to the solutions until DMSO was completely removed. Concentrated micelle solutions were filter-sterilized and stored in aliquots at 4 °C for future use. Drug concentration was determined by UV at 490 nm, based on the calibration curve of free ADR.

Table 2. Particle Size and ζ Potential of the Micelles with Varying Folate Contents

	folate conjugation[a] (%)							
	0 (MA)	1 (FMA1)	2 (FMA2)	5 (FMA5)	10 (FMA10)	25 (FMA25)	50 (FMA50)	100 (FMA100)
particle size[b] (nm)	64.21	65.34	63.79	68.35	69.22	72.51	77.47	91.29
polydispersity index (μ/Γ^2)	0.1018	0.0951	0.1096	0.1232	0.1318	0.1437	0.1661	0.1973
ζ potential (mV)	−0.39	0.11	−0.67	−1.07	−1.98	−2.33	−6.95	−9.25

[a] It was determined by the mixing ratio of folate-conjugated block copolymers to the block copolymers without folate conjugation. [b] The micelles were filter-sterilized using 0.45 μm filter units (Millex-HV, Millipore, Co., Ltd., U.S.A.) prior to the measurements.

In Vitro Cytotoxicity Assay. In order to determine in vitro cytotoxicity of the micelles, a human pharyngeal cancer cell line KB was incubated with FMA, MA, and free ADR in various concentrations, changing exposure time. Exponentially growing KB cells were seeded on a 96-well culture plate (2000 cells/well) and preincubated for 24 h, followed by coincubation with the samples. After 3 and 24 h, cell culture media were replaced with fresh media, and the cells were incubated further for additional 24 h. The number of viable cells was determined by CellTiter-Glo luminescent cell viability assay (n = 8) that provides a convenient, rapid, and sensitive procedure based on quantitation of ATP, which signals the presence of metabolically active cells (*28*).

Flow Cytometric (FCM) Analysis. Cellular uptake of the micelles was analyzed by an EPICS XL Flow Cytometry Systems (Beckman Coulter, U.S.A.) monitoring autofluorescence of ADR accumulated in the cell. KB cells were seeded on a 12-well culture plate (30 000 cells/well) and preincubated for 24 h, followed by coincubation with FMA, MA, and ADR (10 mg/mL) for 3 and 24 h. The cells were then washed three times with PBS, detached by trypsinization, spun down by centrifugation, and dispersed again in PBS for FCM analysis. Data were acquired and processed with the accompanying software (*EXPO 32*).

Surface Plasmon Resonance (SPR) Analysis. Interaction between FBP and the micelles was analyzed by surface plasmon resonance (SPR) measurements using BIAcore 3000 (Biacore, Sweden). FBP was immobilized on the surface of a sensor chip (3 ng/mm^2 of FBP per channel), following the procedures provided by the manufacturer. FBP binding effects of both FMA and MA were evaluated at a flow rate of 10 μL/min with a concentration of 200 μg/mL. The micelles were allowed to flow for 30 min, and all samples were tested by replacing sensor chips on which FBPs were newly immobilized.

Pharmacological Study. Tumor-bearing mice were prepared by transplanting KB cells on the abdominal region of CD-1 nude mice (female, 6-week-old, n = 6, Charles River, Japan). When the tumor volume reached 100 mm^3, the micelles and free ADR as control were intravenously injected in a volume of 0.1 mL/10 g body weight. The drug dose was 10 mg/kg for both free ADR and the micelles (ADR equivalent). After drug injection, the blood, tumor, and major organs (heart, kidney, liver, and spleen) were collected at 0.5, 1, 3, 6, 9, and 24 h, followed by HPLC analysis as previously reported (*19*). Briefly, plasma was separated from the blood, and the tissues were homogenized prior to the measurements. Daunorubicin (DAU) was added to the specimens as an internal standard in 2 μg/mL, depending on sample amount. 200 μL of 10 mM HCl solution was then added to the specimens to cleave drug conjugation, and 1 mL of 100 mM ammonia buffer (pH 9.0) was applied after 24 h incubation. 5 mL of $CHCl_3$/MeOH (2:1) mixed solution was also added to the solution, and ADR and DAU were extracted by vigorous vortexing at 25 °C for 15 min. The organic layer was collected using Pasteur pipets and evaporated at 40 °C after centrifugation (1900 g, 15 min, 4 °C). Dry drugs were redissolved in 100 μL of DMF and injected to RPLC equipped with a μ Bondasphere 5μ C4 300 column and a fluorescence detector (Ex 485 nm, Em 560 nm). The area under the curve of concentration (AUC) vs time was calculated by the trapezoidal rule with the time points of 0.5, 1, 3, 6, 9, and 24 h. The unit for AUC is defined as % dose/mL plasma × h or % dose/g organ × h for the blood or other tissues (tumor, kidney, liver, spleen, and heart), respectively.

Table 3. Time-Dependent Increase in Cytotoxicity and Cellular Uptake of the Micelles (n = 8)[a]

sample	exposure time (h)	IC_{50}[b] (μg/mL ± SD)	relative index[c]	cellular uptake[d] (%)
ADR	3	0.069 ± 0.014	1.97	100.00
	24	0.035 ± 0.011	1	100.00
FMA100	3	0.172 ± 0.017	4.91	92.51
	24	0.041 ± 0.012	1.17	94.95
MA	3	N.D.[e]	N.D.[e]	40.20
	24	0.263 ± 0.013	7.51	82.05

[a] Data were obtained from the eight independent experiments using a human pharyngeal cancer cell KB. [b] IC_{50} means the inhibitory concentration of the drugs required for reducing 50% of cell proliferation. The drug concentration of the micelles was calculated with respect to free ADR equivalents. [c] Relative index means the ratio between the IC_{50} of free ADR after 24 h incubation and the samples. [d] Cellular uptake of the micelles was analyzed by flow cytometric analysis monitoring autofluorescence of ADR accumulated in the cell. [e] N.D. means not determined.

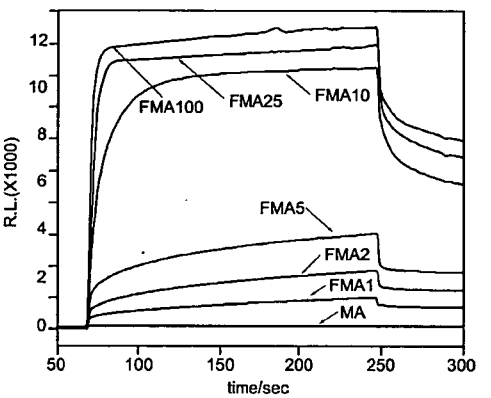

Figure 2. Surface plasmon resonance (SPR) analysis. FBP-binding selectivity of folate-conjugated micelles was evaluated by SPR measurements (eluent, 100 mM phosphate buffer; pH 7.4; flow rate, 10 mL/min; density of folate-binding protein, 3 ng/mm per channel; sample concentration, 200 μg/mL). Folate concentration on the surface of the micelles was varied to determine the optimum substitution rate.

In Vivo Antitumor Activity Evaluation. Tumor-bearing mice were prepared as described above. The micelles were injected from the tail vein three times with a four day interval in various doses (5, 10, 20, and 40 mg/kg). This administration schedule was based on the optimum regimen for free ADR as a control. However, free ADR was applied to the mice in limited doses (5, 10, and 15 mg/kg) due to the serious toxicity. Tumor growth and body weight of mice were checked at every second day. Tumor volume was calculated as volume $V = {}^1/_2 \times LW^2$, where the letters L and W denote the long and short diameters of the tumor tissue. Cancer treatment efficacy was analyzed by a treatment to control (T/C) ratio = $(V_c - V_t) \times 100/V_c$, where

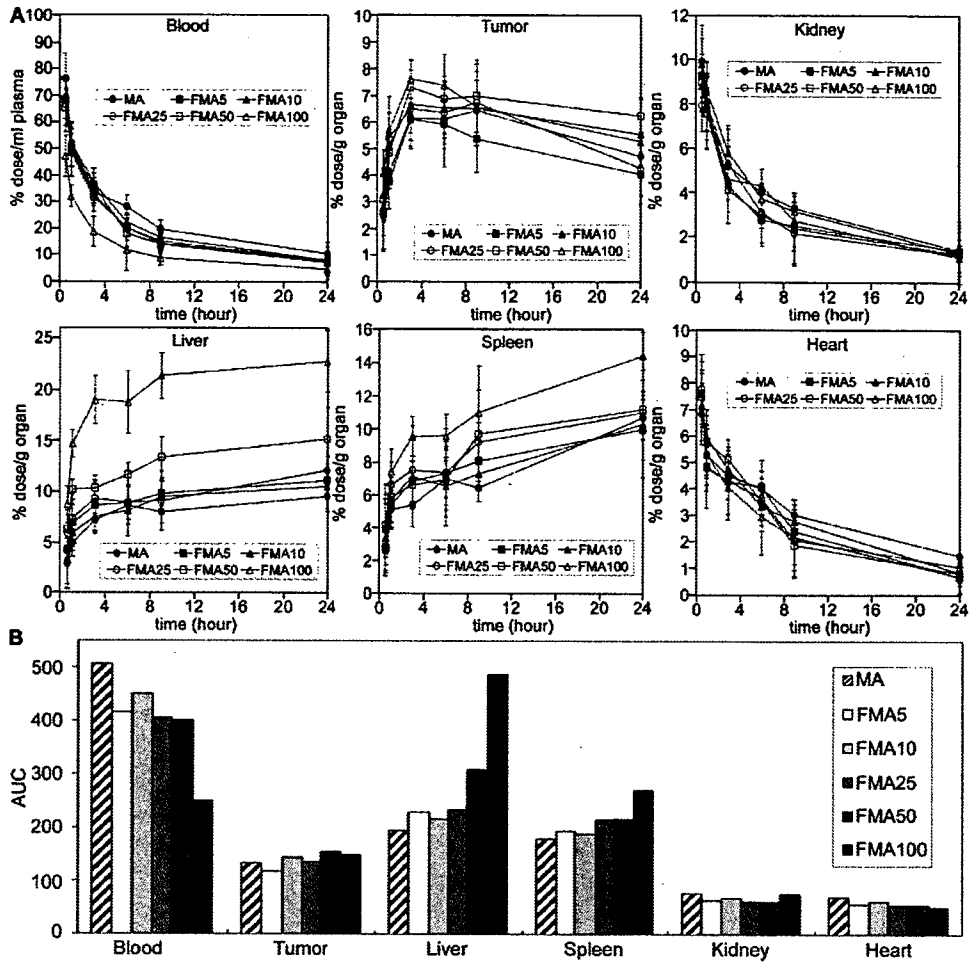

Figure 3. Pharmacokinetic profiles. Distribution of the micelles with varying folate amounts was measured in the blood compartment, tumor tissue, and major organs such as the liver, spleen, kidney, and heart (A). Experiments were carried out using tumor-bearing CD-1 nude mice (female, 6-week-old, $n = 6$) when the tumor volume reached 100 mm^3. Data are expressed as mean and mean ± SEM for relative and absolute values, respectively. Accumulation amounts for each micelle are compared in terms of the areas under the curve of concentration (AUC) vs time up to 24 h time period (B).

V_c and V_t are the mean tumor volumes of the control and the treated mice, respectively. The effective dose (ED) of each micelle was determined as the T/C ratio = 50, which means the average tumor volume of the mice decreased 50% of control values by drug treatments. The toxic dose (TD) was defined as the dose that causes 20% decrease in body weight of the mice after drug injection.

RESULTS AND DISCUSSION

Preparation of the Folate-Conjugated pH-Sensiive Polymeric Micelles (FMA). The molecular weight and composition distributions of self-assembling amphiphilic block copolymers, folate−poly(ethylene glycol)−poly(aspartate-hydrazone-adriamycin) [Fol−PEG−p(Asp-Hyd-ADR)] and α-methoxy-poly(ethylene glycol)−poly(aspartate-hydrazone-adriamycin) [PEG−p(Asp-Hyd-ADR)], were determined by GPC and ^{1}H NMR. Table 1 shows that these block copolymers were successfully prepared with a controlled number of hydrazide groups and ADR. It is noticeable that Fol−PEG−p(Asp-Hyd-ADR) block copolymers did not form any dimers or aggregates after folate conjugation. In addition, most notably, folate was functionalized only at γ-carboxylate position of its glutamate residue in this study by precision synthesis, as we previously reported elsewhere (*25*). This enables every folate molecule that is conjugated to the block copolymers to remain active, distinguishing our system from other folate conjugates. In many studies, folate molecules have been conjugated by using carbodiimide coupling reagents. The folate conjugated in this way is prone to making a mixture of α- and γ-carboxylate-functionalized forms. Because the α-carboxylate-functionalized form of folate loses its activity, the carbodiimide coupling method is substantially accompanied by the problems of undesirable introduction of inactive folate, which induces insufficient conjugation or incorrect quantification of active folate (*23, 24*). To the contrary, herein we can exclude the possibility that folate becomes inactive after conjugation, and therefore, it is able to clearly investigate the effects of folate conjugation on the biological properties of the micelles.

The particle size and ζ potential of the micelles were analyzed by Zetasizer Nano (Malvern, U.K.), and data are summarized in Table 2. Each micelle from Fol−PEG−p(Asp-Hyd-ADR) and PEG−p(Asp-Hyd-ADR) was abbreviated as FMA and MA, which denote folate micellar adriamycin and micellar adriamycin (without folate), respectively. The successive number after the abbreviated term of FMA in some descriptions indicates the mol % of Fol−PEG−p(Asp-Hyd-ADR) block copolymers in the micelles. For instance, FMA10 means that the micelles were prepared from 10% of Fol−PEG−p(Asp-Hyd-ADR) and 90% of PEG−p(Asp-Hyd-ADR) block copolymers. In all cases, the micelles exhibited particle sizes between 60 and 90 nm, while the distribution was narrow and monodisperse. Surface charge

of the micelles became negative, which is probably due to the carboxylic group remaining at the α-position of glutamate of the folate molecule. Although the micelle size slightly increased as folate concentration increased, these data demonstrate that the size and surface charge of the prepared micelles were still suitable for tumor-specific accumulation via the EPR effect after folate conjugation. When the micelle solutions were concentrated, however, aggregation between particles was observed in the case of FMA100. Such aggregation was able to be suppressed by decreasing the folate substitution ratio. Considering that MA (or FMA0) showed no aggregation during concentration, it is most probable that folate substitution increases the local concentration of folate molecules on the micelle surface, and thus, FMA aggregated due to the intermicellar hydrophobic interaction (*29*). Nevertheless, it must be noted that the micelles stably dispersed with 60−90 nm diameter up to 5 mg/mL concentration irrespective of folate substitution ratio. Because a high drug loading content (~30 wt %) is one of the characteristic advantages of the micelles, injecting the micelles above this concentration would not be realistic in terms of determining the injection dosage of ADR whose lethal dose ranges from 12.7 to 13.2 mg/kg. Therefore, it is concluded that the micelles with varying folate contents were stable at a size suitable for systemic drug delivery with sufficient drug concentration.

Folate Conjugation Significantly Increased in Vitro Cytotoxicity and Cellular Uptake of the Micelles. Table 3 shows a change in proliferation of KB cells treated by FMA100, MA, and free ADR and cellular uptake. It is of interest that the 50% inhibitory concentrations (IC_{50}) of cell growth decreased significantly in the case of the micelles by folate conjugation. Notably, cytotoxicity of FMA100 was as high as that of free ADR after 24 h incubation despite their different internalization mechanisms. In our previous studies, it is confirmed that this pH-sensitive micelle, which was designed to selectively release drugs in the intracellular region, requires relatively long exposure time sufficient for inhibiting cell growth (> 10 h). It is because the micelles are required to enter the cell first and to release drug by sensing pH so that the released drugs accumulate in cell nuclei to intercalate with DNA, inducing cell death. In comparison with MA, FMA100 showed efficient cytotoxicity with a short exposure time of 3 h. These results suggest that folate conjugation promotes the interaction between the micelles and the cell. It is generally known that KB cells overexpress folate-binding proteins (FBPs) on the cell membrane, and therefore the FBPs can take up FMA100 to the cell interior efficiently via receptor-mediated endocytosis. Such enhanced cellular uptake probably induced higher cytotoxicity of FMA100 even with short exposure time. This hypothesis was also confirmed by flow cytometric analysis. As also summarized in Table 3, cellular uptake of FMA100 increased by folate conjugation, and such an increment corresponds well with enhanced cytotoxicity. Consequently, it is confirmed that folate conjugation enhanced cytotoxicity of the micelles by increasing cellular uptake and intracellular drug concentration.

FMA Recognized Folate-Binding Proteins (FBPs) Selectively and Strongly. Although in vitro cytotoxicity assay and flow cytometric analysis have proven that high efficacy of FMA was due to the increased intracellular drug concentration, the scientific evidence that elucidates the role of folate in accelerating cellular uptake was still required. In order to confirm the interaction between FMA and folate binding proteins (FBPs), we carried out surface plasmon resonance (SPR) analysis by using a sensor chip on which FBP molecules were immobilized. It is also of great importance to verify how folate concentrations affect FBP binding properties of the micelles, so we prepared FMA with varying folate substitution rates from 100% to 0%.

Table 4. Tumor-Specific Accumulation of the Micelles

sample	blood	tumor	liver	spleen	kidney	heart
AUC[a]						
MA	506.42	132.67	194.45	179.37	76.96	69.48
FMA5	415.53	117.13	229.35	193.65	63.15	57.01
FMA10	450.38	143.60	215.97	187.98	68.45	61.79
FMA25	405.17	135.48	233.33	215.24	61.58	55.59
FMA50	400.76	155.13	308.99	216.80	60.91	54.99
FMA100	250.16	147.86	487.30	270.14	76.10	51.87
			K_b value[b]			
MA	1	0.26	0.38	0.35	0.15	0.14
FMA5	1	0.28	0.55	0.47	0.16	0.15
FMA10	1	0.32	0.48	0.42	0.16	0.15
FMA25	1	0.33	0.58	0.53	0.17	0.16
FMA50	1	0.39	0.77	0.54	0.16	0.15
FMA100	1	0.59	1.95	1.08	0.30	0.25
			tumor to organ ratio[c] (AUC_{tumor}/AUC_{organ})			
MA	–	1	0.68	0.74	1.72	1.91
FMA5	–	1	0.51	0.60	1.81	1.92
FMA10	–	1	0.66	0.76	2.04	2.12
FMA25	–	1	0.58	0.63	1.94	2.16
FMA50	–	1	0.50	0.72	2.48	2.59
FMA100	–	1	0.30	0.55	1.94	2.41

[a] AUC denotes the area under a concentration curve that is obtained from the pharmacokinetic study with time points at 0.5, 1, 3, 6, 9, and 24 h. Values were calculated on the basis of the trapezoidal rule up to 24 h after intravenous injection. The unit for AUC is defined as % dose/mL plasma × h or % dose/g organ × h for the blood or other tissues (tumor, kidney, liver, spleen, and heart), respectively. [b] K_b value is defined as $[K_b = C_{tissue}/C_{blood}]$ where C_{tissue} and C_{blood} are the drug concentrations in the tissue and the blood, respectively. Each K_b value indicates distribution of the drugs in the vascular space ($K_b < 0.1$), extracellular space ($0.1 < K_b < 0.5$), and intracellular space ($0.5 < K_b$). [c] Tumor selectivity of the micelles was determined by calculating the relative accumulated concentrations between the tumor tissues and each organ (AUC_{tumor}/AUC_{organ}).

Figure 2 shows SPR signal intensity versus time for individual micelle samples. The micelles were flowed into the sensor channel for 3 min and rinsed with fresh buffer solution. The signal change indicates that FMA binds promptly and strongly to FBP in various folate contents while MA showed no interaction with FBP. Interestingly, FMA was able to recognize FBP even with 10% folate substitution ratio. However a significant decrease was found in the FBP binding effect between FMA10 and FMA5. In the meantime, the folate substitution rates can be converted from a percent to mol wt % on the basis of the molecular weight of block copolymers and the mixing ratio. It shows that 100% folate substitution ratio corresponds to 16.9 mmol wt % for a single micelle, and FMA10 and FMA5 were calculated to contain 1.7 and 0.8 mmol % of folate molecules, respectively. Therefore, these data revealed that the micelles require only a small quantity of folate to recognize FBPs. Folate is known to have a high affinity for FBP ($K_d < 1$ nM), and such high affinity seems to provide a strong binding property of FMA (*23, 24*).

Optimum Amounts of Folate-Facilitated Tumor Targeting Properties of the Micelles with Long Blood Circulation. The information regarding the relation between the amount of folate and biodistribution of the micelles is of primary importance to determining the compositions of FMA. Such compositions should be considered to maintain the balance between passive and active tumor targeting to realize an ultimate goal of drug delivery systems. For these reasons, we have investigated the biodistribution of FMA by changing folate contents. Figure 3 shows the distribution of the micelles in the blood compartment, tumor tissues, and major organs such as the liver, spleen, kidney, and heart after the intravenous injection. The area under a concentration curve (AUC) shows that the micelles circulated

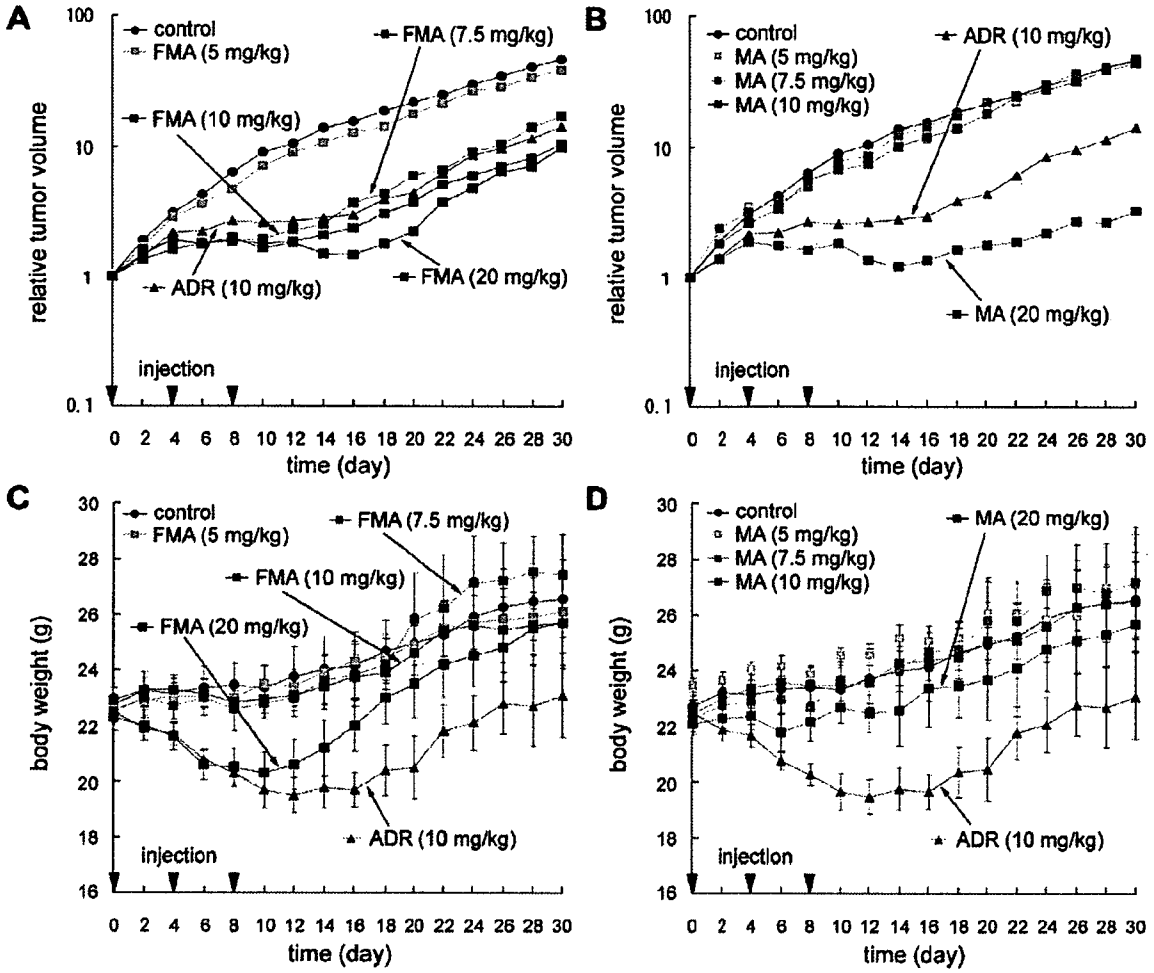

Figure 4. Tumor size and body weight change. The figure shows effective tumor-suppressing activity and low change in body weights over a broad range of injection doses of the folate-conjugated micelles (A and C). It clearly shows that the dose for effective tumor treatments decreased by folate conjugation compared to the micelles without folate, while toxicity remained lower than free drugs (B and D). Administrations were carried out 3 times with a 4 day interval into tumor-bearing CD-1 nude mice (female, 6-week-old, $n = 6$). The micelle doses are shown as ADR equivalents. Data are expressed as mean and mean ± SEM for relative and absolute values, respectively.

in the blood for a long time and their accumulation in tumor tissue increased significantly during the period of 24 h compared to normal organ. In the case of MA, the results correspond well with our previous data that revealed that the intracellular pH-sensitive micelles are characterized by prolonged circulation time in blood and tumor-specific accumulation (*19*). Such characteristic pharmacokinetic properties are considered to result from controlled drug release that can enhance the drug delivery efficiency of the micelles to the solid tumors. Regarding FMA, it is of interest that folate conjugation does not significantly affect the long-term circulation property of the micelles. FMA circulated in the blood for a prolonged time irrespective of folate content. However, the micelle accumulation in the liver as well as in the tumor changes obviously depending on the folate amount. As summarized in Table 4, a clear difference in tumor-specific accumulation was found between FMA and MA. The AUC values for each organ exhibit that FMA with a higher folate content showed a lower tumor-targeting property compared to MA. These results might be due to an increase in accumulation in the liver. Micelle accumulation in the liver was most probably due to the high FBP affinity of the micelles with increased folate concentration. In the meantime, the K_b values, which indicate the drug distribution within inter- and intracellular compartments, show that cellular uptake of FMA increased in tumor cells while remaining low in normal tissues. Nevertheless, the pharmacokinetic data also indicate that the possibility cannot be completely excluded that the micelles underwent nonspecific accumulation in normal organs after folate conjugation. It is not only because the K_b values increased, but also because the tumor to organ ratio (TOR) decreased as folate amounts increased. Accumulation in the liver increased, predominantly decreasing tumor-specific delivery efficiency. One of the previous studies showed that folate conjugation can induce higher hepatic clearance of the conjugates (*30*). Although expression of FBP in the liver would be suggested as a likely reason for the hepatic clearance, we considered that excessive conjugation of folate could increase accumulation of the micelles in normal organs. Therefore, it is concluded that the amount of folate should be carefully determined to facilitate tumor-targeting properties while maintaining long-term blood circulation. This would help us to minimize nonspecific distribution of the micelles in the body. Most noticeably, accumulation of the micelles in the tumor tissues did not significantly differ before and after folate conjugation in terms of pharmacokinetic profile. These findings indicate that the EPR effect seems to still be a major factor in determining the tumor accumulation of drug carriers for active targeting within a 24 h time range. In other words, folate conjugation would mainly affect the distribution of the micelles after extravasation rather than regulate migration of the micelles from the blood compartments to the tumor tissue.

FMA Showed Lower Toxicity and Higher Efficacy than Free Drug. The SPR analysis and biodistribution studies revealed that the optimum amount of folate conjugation is of significant importance to achieve passive and active drug targeting simultaneously. From the obtained data above, we selected FMA10 as the optimum micelle composition for further studies, which was believed to be the most suitable for the best performance in terms of tumor-specific drug delivery. In order to elucidate how folate affects in vivo antitumor activity of the micelles in detail, we have injected FMA, MA, and free ADR into the CD-1 nude mice implanted with human pharyngeal cancer KB cells by changing the dosage. Figure 4 show the changes in tumor size and body weight after drug administration. Free ADR was injected as a control, and it suppressed tumor growth at a dose of 10 mg/kg. The mice were also treated with different doses of free ADR, but there was no effect at 5 mg/kg. At a dose of 15 mg/kg, free ADR showed severe toxicity. These results indicated that free ADR was safe to exhibit the efficacy only within an extremely narrow dose range from 10 to 15 mg/kg. Indeed, body weight reduction was observed even at a dose of 10 mg/kg in the case of free ADR. In contrast to free ADR, MA was able to suppress tumor growth over a broad range of doses ranging from 20 to 40 mg/kg, while its toxicity was significantly low. Such effective and safe antitumor activity of the micelles was consistent with our previous results, which demonstrated the usefulness of intracellular pH-sensitive drug delivery (*18, 19*). Nevertheless, the effective dose (ED) of MA was relatively high compared to free ADR. In case of FMA, however, tumor growth was effectively suppressed with the same dose range of MA, but surprisingly, its ED decreased from 20 to 7.5 mg/kg while toxicity remained low. This value is even lower than the ED of free ADR (10 mg/kg), indicating that the micelles became more effective than free drug by folate conjugation. Therefore, these experimental data clearly elucidate that the drug carrier can show higher efficacy than free drug by optimally balancing passive and active tumor targeting properties as well as controlling drug release profile. It should be emphasized that, although the pharmacokinetic study showed that folate conjugation did not significantly improve the tumor-specific accumulation of the micelles, in vivo antitumor activity experiments clearly show that FMA is more effective to the cancer treatment than free ADR in terms of efficacy and safety. These results also support our hypothesis described above that active targeting seems to mainly affect the distribution profile of the drug carriers within the tumor tissues after extravasation rather than in the blood compartment. It is certain that more studies on this topic should be investigated further in the future. Nevertheless, it is of great importance that the ED of FMA decreased compared to free ADR as well as MA. A lowered dose is obviously beneficial for preventing possible long-term toxicity to the patients. From these aspects, it is concluded that our in vivo studies clearly demonstrate the effects of folate conjugation on active targeting drug delivery.

Folate Conjugation Decreased Effective Dose while Maintaining the Broad Therapeutic Window of the Micelles. The range of drug concentrations that provide the efficacy safely is known as the therapeutic window. If the injection dose is lower than this range, the drug cannot show its efficacy. To the contrary, if the injection dose is higher than the therapeutic window, the drug will induce either acute or chronic toxicity. In this study, animal studies have shown that FMA is more effective and safer than free drugs. In order to provide more objective criteria for evaluating efficacy of FMA, we analyzed antitumor activity of the micelles by calculating a treatment to control (T/C) ratio. Figure 5 exhibits the relation between the T/C ratio and a dosage. Each curve provides information about the tumor-suppressing efficacy of FMA, MA, and free ADR

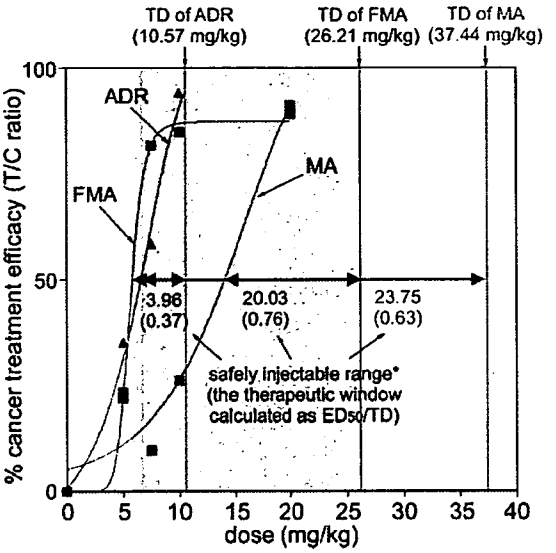

Figure 5. Treatment-to-control (T/C) ratio. Cancer treatment efficacy of the micelles was evaluated by comparing the therapeutic windows of FMA10, MA, and ADR, which were calculated from the ratio of ED_{50} to TD. ED_{50} and TD were defined as the effective dose that induces 50% decrease in tumor volume and the toxic dose that reduces 20% of body weight of mice, respectively. The data show the dose range in which each sample can be safely injected while achieving effective cancer treatments.

with respect to the control. Effective dose (ED) and toxic dose (TD) were defined as the doses that induce 50% of tumor growth (ED_{50}) and reduce 20% of body weight during the treatment, respectively. As drug concentrations increased, tumor growth suppression efficiency increased by all drug formulations. However, when we compare the effective doses, ED_{50} of free ADR is obviously close to its TD while ED_{50} of the micelles remained low compared to their TD. Namely, the safe dose of free ADR was only 3.96 mg/kg, but in contrast, FMA and MA were safely injectable between 20.03 and 23.75 mg/kg, respectively. These values correspond to 5.05- and 5.99-fold broader dose ranges than free drug. In particular, ED_{50} of FMA became lower than that of free ADR, and these results exemplify how active drug targeting is promising for cancer treatment. Most notably, such low toxicity and high efficacy were achieved by determining the optimum amount of folate on the micelle surface.

CONCLUSIONS

Integration of multiple functions into a single nanoparticle can broaden the possibilities of the macromolecular drug delivery systems for their future applications in the clinic. In this study, we have prepared a multifunctional polymeric micelle that is implemented with intracellular pH-dependent drug-releasing functionality and folate-mediated cancer cell targeting property simultaneously. By precision synthesis and preparation of the pH-sensitive micelles with varying folate contents, we were able to elucidate that the ligand-installed micelles for active drug targeting can be more effective than free drug in terms of antitumor activity, safety, pharmacokinetics, and bioavailability. It is of great interest that folate conjugation did not significantly improve the tumor accumulation of the micelles in the body because it induced a prominent increase in accumulation in the liver. However, when folate concentration was adjusted to achieve minimum ligand−receptor interaction, folate-conjugated micelles showed an effective cancer treatment efficiency that was even higher than free drugs as well as the micelles without folate conjugation. These findings clearly demonstrated that the

balance between passive and active drug targeting should be carefully considered to maximize the drug delivery efficiency as well as cytotoxic activity of the polymeric drug carriers.

ACKNOWLEDGMENT

The authors wish to express their thanks for the Project on the Materials Development for Innovative Nano-Drug Delivery Systems from the Ministry of Education, Culture, Sports, Science and Technology (MEXT), Japan.

LITERATURE CITED

(1) Duncan, R. (2006) Polymer conjugates as anticancer nanomedicines. *Nat. Rev. Cancer 6*, 688−701.

(2) Low, P. S., and Antony, A. C. (2004) Folate receptor-targeted drugs for cancer and inflammatory diseases. *Adv. Drug Delivery Rev. 56*, 1055−1058.

(3) Allen, T. M. (2002) Ligand-targeted therapeutics in anticancer therapy. *Nat. Rev. Drug Discovery 2*, 750−763.

(4) Lee, E. S., Na, K., and Bae, Y. H. (2005) Doxorubicin loaded pH-sensitive polymeric micelles for reversal of resistant MCF-7 tumor. *J. Controlled Release 103*, 405−418.

(5) Xu, Z., Gu, W., Huang, J., Sui, H., Zhou, Z., Yang, Y., Yan, Z., and Li, Y. (2005) In vitro and in vivo evaluation of actively targetable nanoparticle for paclitaxel delivery. *Int. J. Pharm. 288*, 361−368.

(6) Oyewumia, M. O., Yokela, R. A., Jaya, M., Coakleyb, T., and Mumper, R. J. (2004) Comparison of cell uptake, biodistribution, and tumor retention of folate-coated and PEG-coated gadolinium nanoparticles in tumor-bearing mice. *J. Controlled Release 95*, 613−626.

(7) Gabizon, A., Horowitz, A. T., Goren, D., Tzemach, D., Shmeeda, H., and Zalipsky, S. (2003) In vivo fate of folate-targeted polyethyleneglycol liposomes in tumor-bearing mice. *Clin. Cancer Res. 9*, 6551−6559.

(8) Jain, R. K. (1998) Delivery of molecular and cellular medicine to solid tumors. *J. Controlled Release 53*, 49−67.

(9) Matsumura, Y., and Maeda, H. (1986) A new concept for macromolecular therapeutics in cancer chemotherapy: mechanism of tumoritropic accumulation of proteins and the antitumor agent Smancs. *Cancer Res. 46*, 6387−6392.

(10) Maeda, H. (2001) SMANCS and polymer-conjugated macromolecular drugs advantages in cancer chemotherapy. *Adv. Drug Delivery Rev. 46*, 169−185.

(11) Minchinton, A. I., and Tannock, I. F. (2006) Drug penetration in solid tumours. *Nat. Rev. Cancer 6*, 583−592.

(12) Kamb, A. (2005) What's wrong with our cancer models? *Nat. Rev. Drug Discovery 4*, 161−165.

(13) Atkins, J. H., and Gershell, L. J. (2002) Selective anticancer drugs. *Nat. Rev. Cancer 1*, 645−646.

(14) Kataoka, K., Harada, A., and Nagasaki, Y. (2001) Block copolymer micelles for drug delivery: design, characterization and biological significance. *Adv. Drug Delivery Rev. 47*, 113−131.

(15) Nishiyama, N., and Kataoka, K. (2006) Nanostructured devices based on block copolymer assemblies for drug delivery: designing structures for enhanced drug function. *Adv. Polym. Sci. 193*, 67−101.

(16) Nishiyama, N., Bae, Y., Miyata, K., Fukushima, S., and Kataoka, K. (2005) Smart polymeric micelles for gene and drug delivery. *Drug Discovery Today: Technol. 2*, 21−26.

(17) Lavasanifar, A., Samuel, J., and Kwon, G. S. (2002) Poly(ethylene oxide)-block poly(L-amino acid) micelles for drug delivery. *Adv. Drug Delivery Rev. 54*, 169−190.

(18) Bae, Y., Fukushima, S., Harada, A., and Kataoka, K. (2003) Design of environment-sensitive supramolecular assemblies for intracellular drug delivery: polymeric micelles that are responsive to intracellular pH change. *Angew. Chem., Int. Ed. 42*, 4640−4643.

(19) Bae, Y., Nishiyama, N., Fukushima, S., Koyama, H., Matsumura, Y., and Kataoka, K. (2005) Preparation and biological characterization of polymeric micelle drug carriers with intracellular pH-triggered drug release property: tumor permeability, controlled subcellular drug distribution, and enhanced in vivo antitumor efficacy. *Bioconjugate Chem. 16*, 122−130.

(20) Mantovani, L. T., Miotti, S., Menard, S., Canevari, S., Raspagliesi, F., Bottini, C., Bottero, F., and Colnaghi, M. I. (1994) Folate binding protein distribution in normal tissues and biological fluids from ovarian carcinoma patients as detected by the monoclonal antibodies MOv18 and MOv19. *Eur. J. Cancer 30A*, 363−369.

(21) Weitman, S. D., Lark, R. H., Coney, L. R., Fort, D. W., Frasca, V., Zurawski, V. R., Jr., and Kamen, B. A. (1992) Distribution of the folate receptor GP38 in normal and malignant cell lines and tissues. *Cancer Res. 52*, 3396−3401.

(22) Hooijberg, J. H., de Vries, N. A., Kaspers, G. J. L., Pieters, R., Jansen, G., and Peters, G. J. (2005) Multidrug resistance proteins and folate supplementation: therapeutic implications for antifolates and other classes of drugs in cancer treatment. *Cancer Chemother. Pharmacol. 58*, 1−12.

(23) Leamon, C. P., and Reddy, J. A. (2004) Folate-targeted chemotherapy. *Adv. Drug Delivery Rev. 56*, 1127−1141.

(24) Lee, R. J., and Low, P. S. (1994) Delivery of liposomes into cultured KB cells via folate receptor-mediated endocytosis. *J. Biol. Chem. 269*, 3198−3204.

(25) Bae, Y., Jang, W.-D., Nishiyama, N., Fukushima, S., and Kataoka, K. (2005) Multifunctional polymeric micelles with folate-mediated cancer cell targeting and pH-triggered drug releasing properties for active intracellular drug delivery. *Mol. BioSyst. 1*, 242−250.

(26) Akiyama, Y., Nagasaki, Y., and Kataoka, K. (2004) Synthesis of heterotelechelic poly(ethylene glycol) derivatives having α-benzaldehyde and ω-pyridyl disulfide groups by ring opening polymerization of ethylene oxide using 4-(diethoxymethyl)benzyl alkoxide as a novel initiator. *Bioconjugate Chem. 15*, 424−427.

(27) Luo, J., Smith, M. D., Lantrip, D. A., Wang, S., and Fuchs, P. L. (1997) Efficient synthesis of pyrofolic acid and pteroyl A azide, reagents for the production of carboxyl differentiated derivatives of folic acid. *J. Am. Chem. Soc. 119*, 10004−10013.

(28) Crouch, S. P., Kozlowski, R., Slater, K. J., and Fletcher, J. (1993) The use of ATP bioluminescence as a measure of cell proliferation and cytotoxicity. *J. Immunol. Methods 160*, 81−88.

(29) Kanie, K., Nishii, M., Yasuda, T., Taki, T., Ujiieb, S., and Kato, T. (2001) Self-assembly of thermotropic liquid-crystalline folic acid derivatives: hydrogen-bonded complexes forming layers and columns. *J. Mater. Chem. 11*, 2875−2886.

(30) Shinoda, T., Takagi, A., Maeda, A., Kagatani, S., Konno, Y., and Hashida, M. (1998) In vivo fate of folate-BSA in non-tumor- and tumor-bearing mice. *J. Pharm. Sci. 87*, 1521−1526.

BC060401P

Density Control of Poly(ethylene glycol) Layer To Regulate Cellular Attachment

Tomomi Satomi,[†,‡,§,||] Yukio Nagasaki,[⊥] Hisatoshi Kobayashi,[§] Hidenori Otsuka,[*,†,‡,§] and Kazunori Kataoka[||,#]

Department of Applied Chemistry, Faculty of Science, Tokyo University of Science, 1-3 Kagurazaka, Shinjuku-ku, Tokyo 162-8601, Japan, Division of Bioengineering and Bioinformatics, Graduate School of Information Science and Technology, Hokkaido University, North 14 West 9, Sapporo 060-0814, Japan, Biomaterials Center, National Institute for Materials Science (NIMS), 1-1 Namiki, Tsukuba, Ibaraki 305-0044, Japan, Division of Clinical Biotechnology, Center for Disease Biology and Integrative Medicine, Graduate School of Medicine, The University of Tokyo, 7-3-1 Hongo, Bunkyo-ku, Tokyo 113-0033, Japan, Graduate School of Pure and Applied Sciences, University of Tsukuba, 1-1-1 Tenodai, Tsukuba, Ibaraki 305-8571, Japan, and Department of Materials Science and Engineering, Graduate School of Engineering, The University of Tokyo, 7-3-1 Hongo, Tokyo 113-8656, Japan

Received August 17, 2006. In Final Form: March 7, 2007

A wide variety of cells usually integrate and respond to the microscale environment, such as soluble protein factors, extracellular matrix proteins, and contacts with neighboring cells. To gain insight into cellular microenvironment design, we investigated two-dimensional microarray formation of endothelial cells on a micropatterned poly(ethylene glycol) (PEG)-brushed surface, based on the relationship between PEG chain density and cellular attachment. The patterned substrates consisted of two regions: the PEG surface that acts as a cell-resistant layer and the exposed substrate surface that promotes protein or cell adsorption. A PEG-brushed layer was constructed on a gold substrate using PEG with a mercapto group at the end of the chain. The density of the PEG-brushed layer increased substantially with repetitive adsorption/rinse cycles of PEG on the gold substrate, allowing marked reduction of nonspecific protein adsorption. These repeated adsorption/rinse cycles were further regulated by using longer (5 kDa) and shorter (2 kDa) PEG to construct PEG layers with different chain density, and subsequent micropatterning was achieved by plasma etching through a micropatterned metal mask. The effects of PEG chain density on pattern formation of cell attachment were determined on micropatterning of endothelial cells. The results indicated that cell pattern formation was strongly dependent on the PEG chain density and on the extent of protein adsorption. Notably, a PEG chain density high enough to inhibit outgrowth of endothelial cells from the cell-adhering region in the horizontal direction could be obtained only by employing formation of a short filler layer of PEG in the preconstructed longer PEG-brushed layer, which prevented nonspecific protein adsorption almost completely. In this way, a completely micropatterned array of endothelial cells with long-term viability was obtained. This clearly indicated the importance of a short underbrushed PEG layer in minimizing nonspecific protein adsorption for long-term maintenance of the active cell pattern. The strategy for cell patterning presented here can be employed in tissue engineering to study cell−cell and cell−surface interactions. It is also applicable for high-throughput screening and clinical diagnostics, as well as interfacing cellular and microfabricated components of biomedical microsystems.

Introduction

Surface engineering techniques for cellular micropatterning are emerging as important tools to clarify the effects of the microenvironment on cellular behavior,[1,2] as cells usually integrate and respond to the microscale environment, such as chemical and mechanical properties of the surrounding fluid and extracellular matrix, soluble protein factors, small signal molecules, and contacts with neighboring cells.[3,4] Furthermore, living cells undergo physiological changes in response to exposure to drugs and environmental perturbations, such as toxins, pathogens, or other agents, and thus high-throughput technologies using whole cells have also been developed.[5−13] To develop this kind of cellular microarray composed of a cell-resistant surface and cell attachment region, micropatterning a protein-repellent surface is important because cellular adhesion and proliferation are regulated by protein adsorption.

* Corresponding author. Address: Hidenori Otsuka, Ph.D., Department of Applied Chemistry, Faculty of Science, Tokyo University of Science, 1-3 Kagurazaka, Shinjuku-ku, Tokyo 162-8601, Japan. Phone: +81-3-5228-8265. Fax: +81-3-5228-8265. E-mail: h.otsuka@rs.kagu.tus.ac.jp.

† Tokyo University of Science.

‡ Hokkaido University.

§ National Institute for Materials Science.

|| Graduate School of Medicine, The University of Tokyo.

⊥ University of Tsukuba.

Graduate School of Engineering, The University of Tokyo.

(1) Whitesides, G. M.; Ostuni, E.; Takayama, S.; Jiang, X.; Ingber, D. E. *Annu. Rev. Biomed. Eng.* **2001**, *3*, 335.

(2) Jeon, N. L.; Baskaran, H.; Detringer, S. K. W.; Whitesides, G. M.; Van de Water, L.; Toner, M. *Nat. Biotechnol.* **2002**, *20*, 826.

(3) Zamir, E.; Katz, B. Z.; Aota, K. M.; Yamada, K. M.; Geiger, B.; Kam, Z. *J. Cell Sci.* **1999**, *112*, 1655.

(4) Geiger, B.; Bershadsky, R.; Pankov, R.; Yamada, K. M. *Nat. Rev. Mol. Cell Biol.* **2001**, *2*, 793.

(5) Stenger, D. A.; Gross, G. W.; Keefer, E. W.; Shaffer, K. M.; Andreadis, J. D.; Ma, W.; Pancrazio, J. J. *Trends Biotechnol.* **2001**, *19*, 304.

(6) Kononen, J.; Bubendorf, L.; Kallioniemi, A.; Barlund, M.; Schraml, P.; Leighton, S.; Torhorst, J.; Mihatsch, M. J.; Sauter, G.; Kallioniemi, O. P. *Nat. Med.* **1998**, *4*, 844.

(7) Ziauddin, J.; Sabatini, D. M. *Nature* **2001**, *411*, 107.

(8) Michalopoulos, G. K.; DeFrances, M. C. *Science* **1997**, *276*, 60.

(9) Anderson, D. G.; Levenberg, S.; Langer, R. *Nat. Biotechnol.* **2004**, *22*, 863.

(10) Revzin, A.; Tompkins, R. G.; Toner, M. *Langmuir* **2003**, *19*, 9855.

(11) Thielecke, H.; Mack, A.; Robitzki, A. *Biosens. Bioelectron.* **2001**, *16*, 261.

(12) Mack, A. R.; Thielecke, H.; Robitzki, A. A. *Trends Biotechnol.* **2002**, *20*, 56.

(13) Otsuka, H.; Hirano, A.; Nagasaki, Y.; Okano, T.; Horiike, Y.; Kataoka, K. *ChemBioChem* **2004**, *5*, 850.

10.1021/la0624384 CCC: $37.00
Published on Web 05/05/2007

A number of approaches to construct protein-repellent and subsequent cell-repellent surfaces have been studied using polymer coating. In fact, there has been a great deal of discussion regarding the molecular properties on the surface, and it is widely believed that effective protein rejection requires the bound polymer to be heavily hydrated, densely packed, neutral, deposited in a thick layer, and conformationally mobile.[14-18] Here, we focus on poly(ethylene glycol) (PEG), one of the most useful polymers to repel protein. Surface modification by PEG leads to a significant reduction in the nonspecific interaction of biological molecules with the surface due to its high degree of hydrophilicity and chain flexibility, inducing an effective exclusion volume effect.[19-22] Most previous studies of surfaces with immobilized PEG have described higher protein-repellent ability with longer chain, resulting in increasing thickness of PEG,[23-27] which is considered to be due to the stronger attenuation of the long-range Lifshitz−van der Waals attraction. However, immobilization of longer PEG chains results in a decrease in chain density due to its larger exclusion volume effect, although it has a sufficiently large separation between the surface and proteins. Conversely, immobilization of shorter PEG chains gives higher density due to its smaller exclusion volume effect, although it has a smaller separation between the surface and proteins. To resolve this controversial issue of the length and density of the PEG layer, we previously reported the development of surface construction using long and short PEG chains; formation of a short, filler layer of PEG in the preconstructed longer PEG-brushed layer prevented nonspecific protein adsorption almost completely.[28] In most studies of this type, a protein-repellent surface will be expected to repel cellular attachment. However, the question of how dense the immobilized PEG chain must be to control cell attachment has still not been answered.

The present study was performed to determine the influence of PEG chain density on cellular attachment directly. For the micropatterning of cells, it is necessary to prevent overgrowth of cells from the cell-adhering pattern; i.e., construction of a cytophobic surface is important for micropatterning. Here, we controlled the modification ratio of long and short PEG chains to construct surfaces with different PEG chain densities, and subsequent micropatterning was achieved by plasma etching through a micropatterned metal mask (ϕ = 100 μm, edge-to-edge spacing of l = 300 μm). The relationship between PEG chain density and cellular attachment is discussed on micropatterning of endothelial cells.

Experimental Section

Materials. Poly(ethylene glycol) (PEG) with a methoxy group at one end and a mercapto group at the other (MeO−PEG−SH) was provided by NOF Corporation (Tokyo, Japan). The molecular weight and polydispersity of PEGs, denoted by PEG2k and PEG5k, were 2096 and 1.05 and 5341 and 1.04, respectively. Gold chips (SIA KIT Au) for SPR measurements were purchased from Biacore AB (Uppsala, Sweden). Human umbilical endothelial cells (HUVEC) were purchased from Cambrex (Cambrex BioScience Walkersville, Inc., Walkersville, MD). HUVECs were cultured in EBM-2 medium (Cambrex). Water used in this study was purified by passing it through a Milli-Q System (Nihon Millipore Co., Tokyo, Japan) until its specific conductivity fell below 0.1 μS cm^{-1}.

1. PEG Immobilization Study. *Preparation of MeO−PEG−SH-Modified Gold Surface.* Immobilization of PEG on the gold sensor chip surface was performed using a surface plasmon resonance (SPR) instrument (Biacore X; Biacore AB, Uppsala, Sweden). Phosphate buffered saline (PBS; pH 7.4, 0.15 M, containing 1 M NaCl) solutions of PEG were injected at a flow rate of 10 μL/min for 10 min at 37 °C under running PBS (pH 7.4, 0.15 M, containing 1 M NaCl). An SPR sensorgram on the gold sensor chip for this adsorption/rinsing (with running PBS) of PEG was monitored, and the amount of immobilized PEG was assessed by the SPR angle shift. PEG solutions with different concentrations were injected on a sensor chip, and then the plateau region for PEG immobilization was determined. To increase (or change) the amount of immobilized PEG, the process of PEG injection was repeated several times according to the reported method.[24] PEGylated surfaces prepared by one, two, and three repetitive injections were denoted as PEG5k(1), PEG5k(2), and PEG5k(3) surfaces, respectively. In a manner similar to the above-repeated process, successive PEGylation with longer and then shorter PEG was carried out. A shorter PEG (PEG2k) as a filler was layered on the surface with the preconstructed longer PEG brushes (PEG5k) by repetitive injection. PEG5k(1) surfaces with three treatments with the filler PEG and PEG5k(2) with four treatments with the filler PEG were denoted as PEG5k(1)/2k(3) and PEG5k(2)/2k(4) surfaces, respectively.

The density of immobilized PEG chains was estimated quantitatively by quartz crystal microbalance (QCM) measurement using an AT-cut gold-sputtered quartz crystal with a resonance frequency of 27 MHz (Initium Inc., Japan). The frequency was recorded after immersing the crystals in the PBS (pH 7.4, 0.15 M, containing 1 M NaCl) at 37 °C. After baseline stabilization, PEG solutions (PEG5k, PEG2k) were injected at a concentration of 0.01 mg/mL, which was optimized above in the same repetitive manner as in SPR measurement (PEG5k(3), PEG5k(1)/2k(3), PEG5k(2)/2k(4)).

Surface Characterization. The wettability of all PEGylated surfaces was estimated from the static and dynamic contact angle measurements (CA-W contact angle meter; Kyowa Interface Science Co., Ltd., Tokyo, Japan).[29] Gold and PEGylated gold surfaces were constructed on glass substrates as described in detail in the section describing the cell culture study (see "Construction of PEGylated surface"). Water-in-air and air-in-water systems were applied in the static contact angle measurements. Water-in-air system measurement was performed by a sessile droplet technique, where a water droplet (Milli-Q quality) was placed on the sample surface at 25 °C. The air-in-water system procedure followed the captive bubble technique, where the sample surface was immersed in water maintained at 25 °C and a small air bubble was placed on the sample surface from the bottom using a curved needle. The contact angle of each surface was measured on 10 spots, and the obtained values were averaged.

For dynamic contact angle measurements, the advancing (θ_{adv}) and receding (θ_{rec}) contact angles were obtained by extending and then contracting the volume (5.9 μL) of the water droplet using a motor-driven syringe at a rate of 1.88 μL/s for 3.1 s. The extending/contracting droplet was monitored with a CCD camera; each picture was captured every 67 ms, and 24 images were taken for both θ_{adv} and θ_{rec}, when the water droplet volume was changed at 1.88 μL/s. The contact angles were evaluated from video printouts of the droplet.

(14) Lee, J. H.; Kopeckova, P.; Kopecek, J.; Andrade, J. D. *Biomaterials* **1990**, *11*, 455.
(15) Desai, N. P.; Hubbell, J. A. *Macromolecules* **1992**, *25*, 226.
(16) Bergstrom, K.; Osterberg, E.; Holmberg, K.; Riggs, J. A.; Van Alstime, J. M.; Schuman, T. P.; Burns, N. L.; Harris, J. M. *Colloids Surf. A* **1993**, *77*, 159.
(17) Sofia, S. J.; Premnath, V.; Merrill, E. W. *Macromolecules* **1998**, *31*, 5059.
(18) Osterberg, E.; Bergstrom, K.; Holmberg, K.; Schuman, T. P.; Riggs, J. A.; Burns, N. L; Van Alstine, J. M.; Harris, J. M. *J. Biomed. Mater. Res.* **1995**, *29*, 741.
(19) Mori, Y.; Nagaoka, S.; Takiuchi, H.; Kikuchi, T.; Noguchi, N.; Tanzawa, H.; Noishiki, Y. *Trans. Am. Soc. Artif. Internal Organs* **1982**, *28*, 459.
(20) Bergstrom, K.; Osterberg, E.; Holmberg, K.; Hoffman, A. S.; Schuman, T. P.; Kozlowski, A.; Harris, J. M. *J. Biomater. Sci. Polym. Ed.* **1994**, *6*, 123.
(21) Harris, J. M., Ed. *Poly(ethylene glycol) Chemistry, Biotechnical and Biomedical Applications*; Plenum Press: New York, 1992.
(22) Glass, J. E., Ed. *Hydrophilic Polymers, Performance with Environmental Acceptance*; American Chemical Society: Washington DC, 1996.
(23) Prime, K. L.; Whiteside, G. M. *J. Am. Chem. Soc.* **1993**, *115*, 10714.
(24) Gombotz, W. R.; Guanghui, W.; Horbett, T. A.; Hoffman, A. S. *J. Biomed. Mater. Res.* **1991**, *25*, 1547.
(25) Lee, J.; Martic, P. A.; Tan, J. S. *J. Colloid Interface Sci.* **1989**, *131*, 252.
(26) Jeon, S. I.; Andrade, J. D.; de Gennes, P. G. *J. Colloid Interface Sci.* **1991**, *142*, 159.
(27) Roosjen, A.; van der Mei, H. C.; Busscher, H. J.; Norde, W. *Langmuir* **2004**, *20*, 10949.
(28) Uchida, K.; Otsuka, H.; Kaneko, M.; Kataoka, K.; Nagasaki, Y. *Anal. Chem.* **2005**, *77*, 1075.
(29) Otsuka, H.; Nagasaki, Y.; Kataoka, K. *Biomacromolecules* **2000**, *1*, 39.

Protein Adsorption Study. A protein adsorption study, which is an important reference for cell attachment, was performed using SPR equipment. Before the protein adsorption study, three types of PEGylated surface were constructed on a gold sensor chip in the same manner as described above: PEG5k(3), PEG5k(1)/2k(3), and PEG5k(2)/2k(4). And then protein adsorption was estimated by flowing 100 μL of serum-containing medium (EBM-2 medium to culture HUVEC) at a flow rate of 10 μL/min at 37 °C under running PBS (pH 7.4, 0.15 M) on the three types of PEGylated surface and native gold surface. The magnitude of the SPR angle shift by this injection was measured from the data taken from the final part of the curve after the surfaces were rinsed, and assessed as the amount of protein adsorbed. As a control, protein adsorption on a bare gold surface was examined.

2. Cell Culture Study. *Construction of PEGylated Surface.* Glass slides were etched with a boiling mixture of 50% (v/v) sulfuric acid and 50% (v/v) hydrogen peroxide for 30 min and then rinsed thoroughly with water. At 10^{-6} Torr, a 10 Å film of chromium was vapor-deposited at a rate of 0.1 Å/s onto the glass substrate. A 200 Å film of gold was then vapor-deposited on top of it at a rate of 0.1 Å/s. PEGylated surfaces were prepared on the gold films in the same manner as described for SPR measurements. PBS (pH 7.4, 0.15 M, containing 1 M NaCl) solutions of PEG5k (0.01 mg/mL) and PEG2k (0.01 mg/mL) were prepared. Then, PEG solutions with the appropriate conditions were retained on the gold film for 30 min to construct the PEGylated surfaces described above (PEG5k(3), PEG5k(1)/2k(3), PEG5k(2)/2k(4)). The plates were washed with Milli-Q water between each PEGylation, for 5 min each time.

Micropatterning of PEGylated Surface. The micropattern on the PEGylated surfaces were obtained by $N_2 + H_2$ plasma etching using a metal mask with holes 100 μm in diameter spaced 300 μm apart. After construction of a 2-well plastic chamber (Falcon BD) on the glass thus prepared, all samples were sterilized with ethylene oxide gas.

Cell Culture Study. HUVECs were seeded onto the micropatterned PEGylated surface at a cell density of 1×10^6 cells/mL. Cells were cultured at 37 °C in a humidified atmosphere of 5% CO_2. An EBM-2 medium was used for cultivation and was exchanged every 2 days.

Results and Discussion

Micropatterned PEGylated substrates with two-dimensional arrays of plasma-etched circular domains (ϕ = 100 μm) were prepared by sequential immobilization of PEG possessing a mercapto group at the end of the chain on the gold substrate, followed by plasma etching through a metal mask pattern with circular holes. The PEGylated region on the patterned substrate acts to repel proteins and thus inhibits cell adhesion. Proteins are expected to adsorb from the serum-containing medium onto the plasma-etched circular domains, exposing the base gold surface.

1. PEG Immobilization Study. The surface properties of the PEG coating were studied in detail to estimate protein adsorption and subsequent cell culture study on PEGylated surfaces. First, PBS solutions of various concentrations of PEG including 1 M NaCl were injected onto the gold surface using an SPR instrument to optimize immobilized concentration on a sensor chip. Use of high ionic strength buffer caused an increase in the amount of immobilized PEG, due to the appreciably reduced solubility of PEG in concentrated buffer solution.[30] The changes in SPR angle at each concentration of PEG5k are plotted in Figure 1. The results confirmed that the amount of immobilized PEG increased with increases in the injected PEG concentration; saturation was observed at PEG concentrations over 0.01 mg/mL, suggesting that the amount of possible immobilization on the gold surface is constant with injection of PEG above this concentration. There were no significant differences in this PEG immobilization study between PEG2k and PEG5k. Therefore, immobilization of PEG

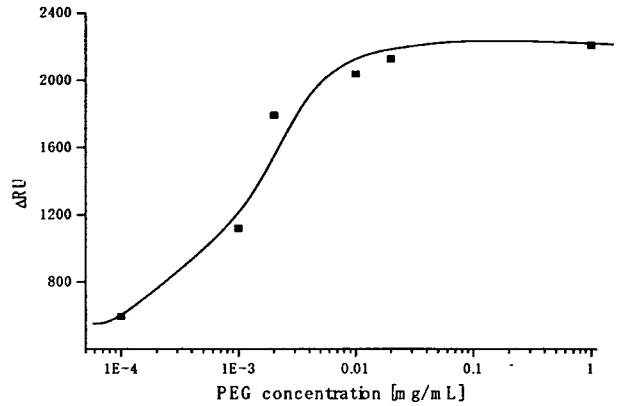

Figure 1. PEG immobilization as a function of PEG concentration. Flow rate, 10 μL/min; running buffer, PBS (pH 7.4, 0.15 M, containing 1 M NaCl); sample, PEG (M_w: 5k)/PBS (0.15 M, pH 7.4, containing 1 M NaCl) solution; sample injection, 100 μL.

on the gold surface was performed with 0.01 mg/mL PEG solution. Three types of PEG immobilization (PEG5k(3), PEG5k(1)/2k-(3), PEG5k(2)/2k(4), as described in the experimental section) were performed at this concentration, as shown in SPR sensorgrams (Figure 2). After first treatment with PEG5k, the sensor surface was washed under running buffer to remove noncovalently adsorbed PEG. The sensor chip was then treated again with a solution of PEG5k. This cycle of adsorption/rinsing of PEG5k was repeated several times. Eventually, the total SPR angle shift was amplified by increasing the number of treatment cycles to three, indicating that repetitive treatment with PEG5k was effective in increasing the density of PEG (PEG5k(3)). Notably, this trend became even more significant following additional treatment of the PEG5k surface with shorter PEG (PEG2k), as shown in Figure 2b,c. We planned to increase the surface brush density by PEG2k, retaining the PEG5k brush surface character. Sensorgrams showed a number of interesting findings. First, immobilization of long-chain PEG (PEG5k(1)) increased markedly with changes in SPR angle (Figure 2a–c). However, the extent of the shift decreased with the second injection of long-chain PEG (PEG5k(2)) (Figure 2a,c), and little change was seen on the third injection of long-chain PEG (PEG5k-(3)) (Figure 2a). On the other hand, immobilization of short-chain PEG (PEG2k(1)) after long-chain PEG resulted again in marked changes (Figure 2b,c). These results suggested that long-chain PEG5k can hardly penetrate into the preconstructed longer PEG-brushed layer due to its exclusion volume effect, while short-chain PEG2k appreciably filled the gap in the preconstructed longer PEG layer. It should be noted that SPR sensorgrams showed a steep increase curve in PEG2k(1), as shown in Figure 2b,c, indicating the importance of a short underbrushed PEG layer in increasing the PEG chain density.

To confirm that these SPR angle changes are reflected directly in the amount of immobilized PEG, QCM measurement was performed in the same manner as SPR (Table 1). The average value of total frequency shift after PEG injection is given as Δf in Table 1. PEG5k(2)/2k(4) surface showed the largest frequency shift, and PEG5k(1)/2k(3) surface also showed around 2000 Hz in frequency shift. On the other hand, PEG5k(3) surface showed around 1400 Hz in total frequency shift. Thus, PEG5k surface mixed with PEG2k showed larger mass change than only PEG5k chain immobilization, which suggested that more PEG chains were immobilized in PEG5k and PEG2k mixed surface. This result also indicated a significant role of a short underbrushed PEG layer in increasing the PEG chain density. On QCM

(30) Emoto, K.; Harris, J. M.; Alstine, M. V. *Anal. Chem.* **1996**, *68*, 3751.

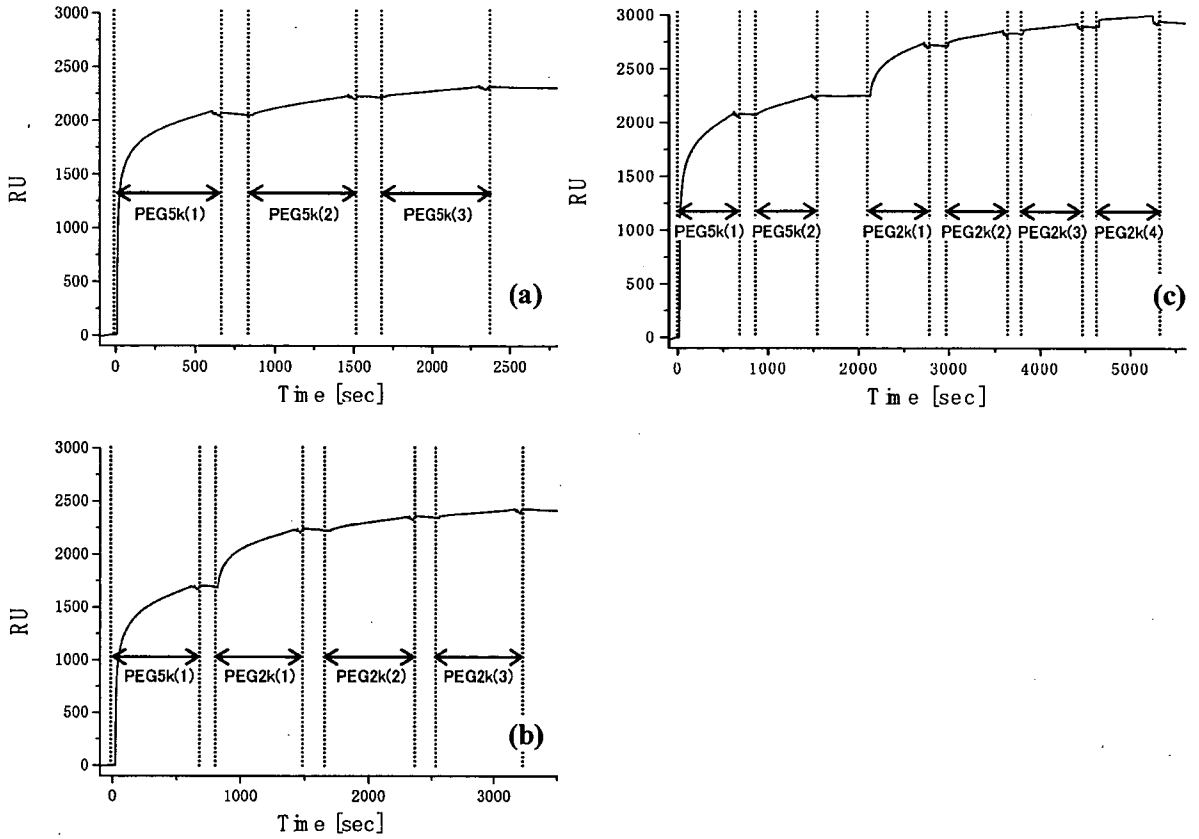

Figure 2. Sensorgrams of PEG immobilization on gold surfaces. (a) PEG5k(3), (b) PEG5k(1)/2k(3), and (c)PEG5k(2)/2k(4). Flow rate, 10 μL/min; running buffer, PBS (0.15 M, pH 7.4, containing 1 M NaCl); sample, 0.01 mg/mL of PEG (M_w: 5k or 2k)/PBS (0.15 M, pH7.4, containing 1 M NaCl) solution; sample injection, 100 μL for each time point.

Table 1. Comparison of Three Types of PEG Immobilization Measured by QCM: Δf is the Average of Total Frequency Shift after PEG Immobilization (n = 3)

PEG surfaces	Δf (Hz)	±S.D.
5k(3)	1382.8	118.6
5k(1)/2k(3)	1922.8	92.70
5k(2)/2k(4)	2144.7	81.74

measurement, the PEG5k(2)/2k(4) surface was determined to have the highest PEG chain density, while PEG5k(3) had the lowest.

The static wettability of the surface coated with PEG was estimated in both air and water by contact angle measurement (Figure 3). In the water-in-air measurement, the coating of PEG on the gold substrate significantly increased its wettability, as indicated by a decrease in the static contact angle (~30°). A similar trend was observed in the air-in-water measurement and the effect of PEG density on wettability was more pronounced, showing progressively increasing contact angle with increasing PEG chain density. Note that the increase in contact angle corresponds to an increase in wettability for the air-in-water system. As the accuracy of contact angle is ±2°, as shown by Zisman and co-worker,[31] significant differences could be seen between PEG surfaces. Furthermore, advancing/receding contact angles and hysteresis were measured on each PEG surface to estimate the dynamics of the uppermost surface in detail (Figure 4). In receding contact angles, each PEG surface showed a small value of around 15−20° and there was little difference between surfaces. On the other hand, critical differences were observed

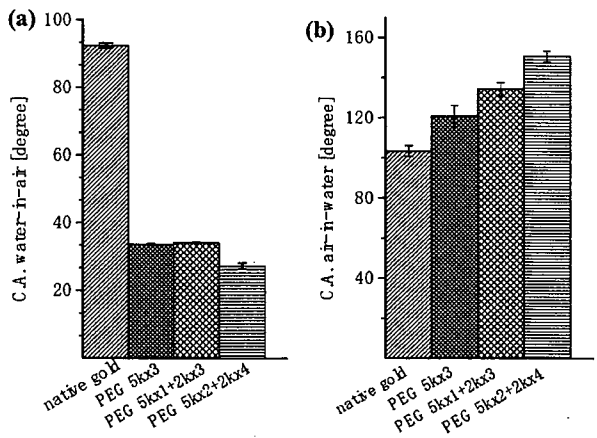

Figure 3. Static water contact angles on PEGylated gold surface. (a) Water-in-air system; (b) air-in-water system.

in advancing contact angles. PEG5k(3) and PEG5k(1)/2k(3) surfaces had around 30°, while the value for the PEG5k(2)/2k(4) surface was almost half. As PEG surfaces are easy to hydrate and show good water retentivity, once they became wet, receding contact angles showed small values in all PEG surfaces, resulting in little difference in receding contact angle. In contrast, significant differences were observed in advancing contact angles, indicating that the PEG5k(2)/2k(4) surface has the greatest wettability in the dry to wet state as compared with the other PEG surfaces examined. Hysteresis indicated differences between PEG5k(2)/2k(4) surfaces and the other surfaces according to its high surface free energy. When the water droplet extends, the surface with

(31) Fox, H. W.; Zisman, W. A. *J. Colloid Sci.* **1950**, *5*, 514.

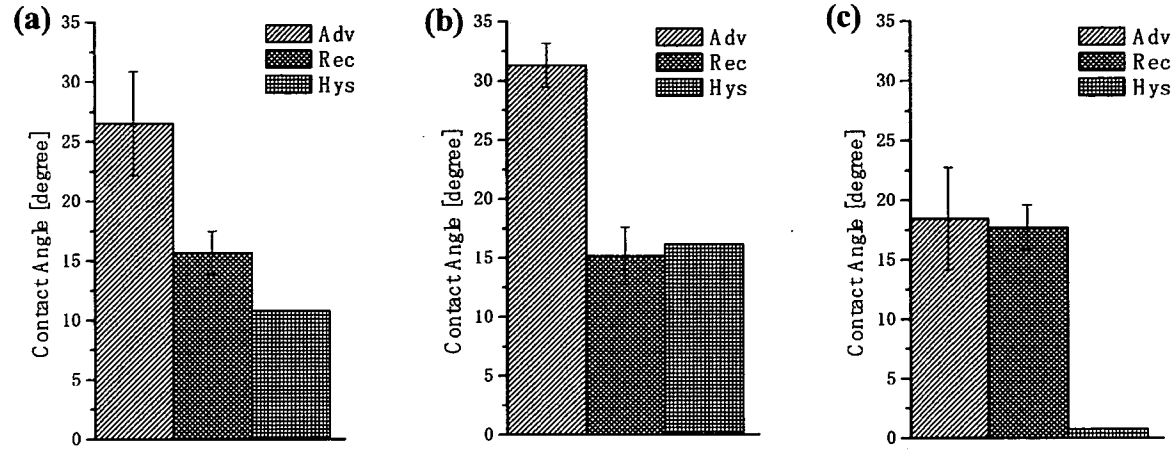

Figure 4. Dynamic water contact angles on PEGylated gold surfaces. (a) PEG5k(3), (b) PEG5k(1)/2k(3), and (c) PEG5k(2)2k(4).

a high surface free energy facilitates penetration of water, aiding in water droplet spreading, while the surface prevents the water droplet from receding when it contracts. Accordingly, the observations of the present study suggested that the PEG5k-(2)/2k(4) surface is the most hydrophilic and has a high surface free energy due to its high PEG chain density. Furthermore, the chain density is reported to have the relation with other parameters including the thickness and conformation of PEG layer.[23−27,32,33] The PEG chains (5k and 2k) are more well-oriented in this surface since the short, filler-like PEG2k chains will enhance the lateral interactions (e.g., hydrogen bonding and van der Waals force) between the PEG chains. This will likely result in much enhanced water affinity/penetration capability in PEG chains during the advancing angle measurement. Therefore, only small hysteresis value will be found on a PEG5k(2)/2k(4) surface.

Nonspecific protein adsorption from the culture medium for HUVEC was estimated on each PEG-coated surface to estimate the cytophobicity of PEGylated surfaces because the adsorbed proteins are responsible for subsequent cell adhesion. On bare gold as a control, the SPR angle shift due to the nonspecific adsorption of protein was 2927.4 RU, when a serum-containing cell (HUVEC) culture medium (EBM-2) was passed over the surface for 10 min at a flow rate of 10 μL/min. In contrast, PEG-coated surfaces clearly reduced protein adsorption (Figure 5). Figure 5 also shows a comparison of protein adsorption on the three types of PEG surface. The SPR angle shift was 676.5, 350.8, and 218.0 RU on PEG5k(3), PEG5k(1)/2k(3), and PEG 5k(2)/2k(4) surfaces, respectively. The PEG5k(2)/2k(4) surface showed the greatest degree of inhibition of protein adsorption from the medium, suggesting that the inhibitory effect of nonspecific protein adsorption was the highest for this surface among those studied. The physicochemical properties of PEG surfaces described above indicate that PEG surfaces with higher immobilized PEG chain density have greater ability to repel proteins. Based on these results, it was concluded that shorter PEG, viz. an underbrushed layer to increase the PEG surface density, played a substantial role in minimizing nonspecific protein adsorption. Other workers have also proposed that PEG mixtures, which are polydisperse with respect to molecular weight, are more efficacious than single molecular weights. Mixed PEGs were shown to have greatest efficacy in steric stabilization of colloidal particles and in protein repellency.[34,35] The PEG5k-

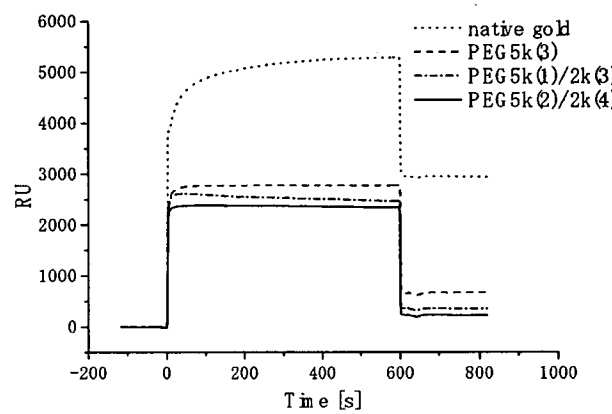

Figure 5. Sensorgrams of injection of serum-containing cell culture medium (EBM-2 medium to culture HUVEC) on native gold and each PEGylated surfaces. Flow rate, 10 μL/min; running buffer, PBS (pH 7.4, 0.15 M); sample injection volume, 100 μL.

(2)/2k(4) surface with the highest PEG chain density was expected to have the highest cytophobicity.

2. Cell Culture Study. Gold surfaces were coated with PEG to inhibit nonspecific protein adsorption and were expected to act as cytophobic surfaces for subsequent cell patterning. The PEG-coated gold substrates were micropatterned by plasma etching ($N_2 + H_2$) through a metal mask pattern with ϕ100 μm circular holes separated by 300 μm (edge-to-edge distance), and cell culture dishes were then set onto these surfaces (2 × 2 cm). Microscopic images following seeding of HUVEC on the surfaces are shown in Figure 6. On PEG5k(3) surfaces with lower PEG chain density as suggested by physicochemical studies, seeded HUVEC showed disorganized cellular attachment regardless of micropatterned substrate (Figure 6a). On the other hand, the PEG5k(1)/2k(3) surface (Figure 6b) and PEG5k(2)/2k(4) surface (Figure 6c) showed patterned cell attachment due to the suggested higher PEG chain density compared with that of the PEG5k(3) surface, although cells that had overgrown beyond the pattern were still observed on PEG5k(1)/2k(3) surfaces. The results of cultivation of HUVECs for 1 week are shown in Figure 6d−f. Arrayed cellular attachment was observed only on the PEG5k-(2)/2k(4) surface (Figure 6f). In contrast, the HUVECs began to bridge across multiple islands on the PEG5k(1)/2k(3) surface (Figure 6e) and this bridging was more pronounced to form a complete cell sheet on the PEG5k(3) surface (Figure 6d). It is

(32) Harder, P.; Grunze, M.; Dahint, R.; Whitesides, G. M.; Laibinis, P. E. *J. Phys. Chem.* **1998**, *102*, 426.
(33) Zhu, B.; Eurell, T.; Gunawan, R.; Leckband, D. *J. Biomed. Mater. Res.* **2001**, *56*, 406.
(34) Stenkamp, V. S.; Berg, J. C. *Langmuir* **1997**, *13*, 3827.
(35) Pavey, K. D.; Olliff, C. J. *Biomaterials* **1999**, *20*, 885.

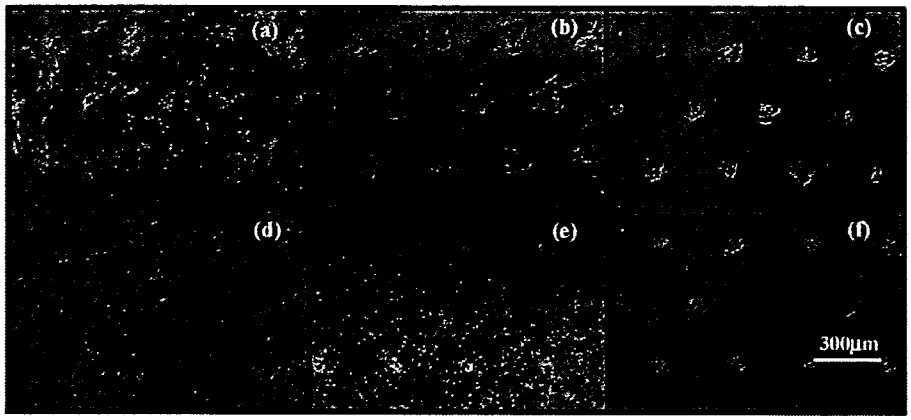

Figure 6. Microscopic image of cell seeding study. After 1 day of culture of HUVEC on micropatterned (a) PEG5k(3) surface, (b) PEG5k-(1)/2k(3) surface, and (c) PEG5k(2)/2k(4) surface. After 1 week of culture of HUVEC on micropatterned (d) PEG5k(3) surface, (e) PEG5k-(1)/2k(3) surface, and (f) PEG5k(2)/2k(4) surface.

clear that PEG chain density affects pattern recognition in cell attachment. The threshold density for HUVEC bridging seems to exist on the surface between PEG5k(3) and PEG5k(2)/2k(4). Cells overgrew beyond the pattern on weak protein-repellent surfaces. In addition, when overgrown cells grew sufficiently close together, bridging occurred between overgrown cellular patterns. Attached patterns eventually resulted in sheet formation. As described above, no pattern recognition of cell attachment was seen on the surfaces coated only with long-chain PEG (PEG5k(3)) because of its lower inhibitory effect on nonspecific protein adsorption. In contrast, cell array formation was observed by constructing long- and short-chain PEG mixed surfaces. Furthermore, PEG5k(2)/2k(4) surfaces showed the least non-specific cell attachment in contrast to some nonspecific cell attachment and bridging of cellular islands on PEG5k(1)/2k(3) surfaces. SPR results indicated that cell-adhesive proteins are greatly repelled on PEG5k(2)/2k(4) surfaces to promote pattern recognition of cell attachment. Some cell attachment between cellular islands was confirmed on PEG5k(3) and 5k(1)/2k(3) surfaces after 1 day in culture, and the attached cells extended toward each other and bridging occurred across cellular islands. Bridged cellular patterns grew everywhere on the surface and eventually formed a complete cell sheet. As the first cell attachment on the cytophobic region depends on the ability of the surface to repel protein, surfaces with lower PEG chain density (PEG5k(3) or PEG5k(1)/2k(3)) resulted in cell attachment and cell sheet formation. Thus, the results of the cell culture study agreed well with the surface properties, suggesting that PEG chain density played a critical role in micropatterned cell attachment.

Conclusions

To gain insight into the design of cellular microenvironments, we examined the micropatterning of endothelial cells on microfabricated gold substrates coated with PEG brushes in terms of the relationship between PEG chain density and cellular attachment. A PEG-brushed layer was constructed on a gold substrate using PEG with a mercapto group at the chain end. After treatment with longer chain PEG with a molecular weight of 5000, shorter chain PEG (2000) was introduced onto the gold substrate to modulate the chain density. In this way, PEGylated surfaces with different chain densities were produced, and subsequent micropatterning was achieved by plasma etching through a micropatterned metal mask. The results indicated that cell pattern formation was strongly dependent on both the PEG chain density and the extent of protein adsorption, as evidenced by physicochemical and biological characterization of PEGylated surfaces using SPR, QCM, and static/dynamic contact angle measurements. Cell micropatterning showed long-term retention only on the surfaces with greater disparity between cytophobic and cytophilic regions. Notably, a PEG chain density sufficiently high to inhibit outgrowth of endothelial cells beyond the cytophilic gold region to the cytophobic PEGylated region could be obtained only on the mixed PEG chain-tethered surface, which achieved almost complete prevention of nonspecific protein adsorption. These observations clearly indicated that shorter PEG, viz. an underbrushed PEG layer to increase the PEG surface density, played a substantial role in minimizing nonspecific protein adsorption and long-term maintenance of the active cell pattern. It should be noted that the precise control of surface properties in single-molecule order directly affected micropatterned cellular attachment. Therefore, we envision the cellular micropatterning technique presented here becoming a valuable tool for the control of cell−surface and cell−cell interactions on a micrometer scale and to evaluate local effects of engineered microenvironments on cellular behavior. The surface fabrication technique studied here is a promising technology for the development of tissue/cell-based biosensors and in the field of tissue engineering.

Acknowledgment. Microfabrication using the plasma etching technique was conducted at the National Institute for Materials Science (NIMS), Japan, with assistance from Dr. Y. Horiike. Financial support for this work was partly provided by Special Coordination Funds for Promoting Science and Technology and also supported by Research Promotion Bureau under contract nos. 15-99 and 15-396, both from the Ministry of Education, Culture, Sports, Science, and Technology (MEXT), Japan. Part of this work was also supported financially by a Grant-in-Aid for Research on Health Sciences for Drug Innovation (KH71066), Ministry of Health, Labor, and Welfare of Japan, and The New Energy and Industrial Technology Development Organization (NEDO).

LA0624384

Gene Therapy (2007) 14, 1029–1038

www.nature.com/gt

ORIGINAL ARTICLE

Biocompatible micellar nanovectors achieve efficient gene transfer to vascular lesions without cytotoxicity and thrombus formation

D Akagi[1,2], M Oba[3], H Koyama[3], N Nishiyama[4], S Fukushima[2], T Miyata[1], H Nagawa[1] and K Kataoka[2,4,5]

[1]*Division of Vascular Surgery, Department of Surgery, Graduate School of Medicine, The University of Tokyo, Bunkyo-ku, Tokyo, Japan;* [2]*Department of Materials Engineering, Graduate School of Engineering, The University of Tokyo, Bunkyo-ku, Tokyo, Japan;* [3]*Department of Vascular Regeneration, Graduate School of Medicine, The University of Tokyo, Bunkyo-ku, Tokyo, Japan;* [4]*Division of Clinical Biotechnology, Center for Disease Biology and Integrative Medicine, Graduate School of Medicine, The University of Tokyo, Bunkyo-ku, Tokyo, Japan and* [5]*Center for NanoBio Integration, The University of Tokyo, Bunkyo-ku, Tokyo, Japan*

Gene therapy, a promising treatment for vascular disease, requires appropriate gene vectors with high gene transfer efficiency, good biocompatibility and low cytotoxicity. To satisfy these requirements from the approach of nonviral vectors, a novel block copolymer, poly(ethylene glycol) (PEG)-block-polycation, carrying ethylenediamine units in the side chain (PEG-b-P[Asp(DET)]) was prepared. PEG-b-P[Asp(DET)] formed a polyplex micelle through polyion complex formation with plasmid DNA (pDNA). The PEG-b-P[Asp(DET)] polyplex micelle showed efficient gene expression with low cytotoxicity against vascular smooth muscle cells in vitro. *It also showed reduced interactions with blood components, offering its feasibility of gene delivery via the vessel lumen. To evaluate* in vivo *gene transfer efficiency for vascular lesions, PEG-b-P[Asp(DET)] micelle was instilled into rabbit carotid artery with neointima by an intravascular method, and expression of the reporter gene in vascular lesions was assessed. Polyplexes from homopolymer P[Asp(DET)] and branched polyethyleneimine (BPEI) were used as controls. Ultimately, only the polyplex micelle showed appreciable gene transfer into vascular lesions without any vessel occlusion by thrombus, which was in strong contrast to BPEI and P[Asp(DET)] polyplexes which frequently showed occlusion with thrombus. These findings suggest that the PEG-b-P[Asp(DET)] polyplex micelle may have promising potential as a nonviral vector for the treatment of vascular diseases.*
Gene Therapy (2007) **14**, 1029–1038. doi:10.1038/sj.gt.3302945; published online 26 April 2007

Keywords: *gene delivery; non-viral gene vector; polyplex micelle; vascular disease; intimal hyperplasia; biocompatibility*

Introduction

Local gene delivery is a promising approach for the treatment of refractory vascular disease. Previous studies have presented a variety of strategies for transferring therapeutic genes to the vascular wall.[1,2] Viral vectors, such as adenovirus vector, have been commonly utilized in these strategies, because the gene transfer efficiency with a viral vector is generally higher than that by other nonviral methods. However, the clinical use of viral vectors has considerable limitations with respect to safety.[3,4] For therapeutic application of gene delivery to the vascular wall, it is, therefore, desirable to develop a nonviral vector with safety and reasonable efficiency of gene transfer.

Several cationic polymers (polycations), which form a polyion complex with DNA (polyplex) and then promote introduction of the DNA into cells, have been widely used as nonviral vectors in several studies *in vitro*.[5,6] However, positively charged polyplexes might potentially induce cytotoxicity and form aggregates in biological media containing plasma proteins, indicating that *in vivo* applications of such polyplexes might be markedly restricted.[7,8] To resolve this issue, we recently designed biocompatible nonviral vectors constructed from newly synthesized cationic block copolymer.[9] The block copolymer thus synthesized is characterized by tandem alignment of a hydrophilic poly(ethylene glycol) (PEG) segment and a cationic polyaspartamide segment carrying an ethylenediamine unit at the side chain (PEG-*b*-P[Asp(DET)]) (Figure 1a),[10] leading to the formation of stable and biocompatible polyplex micelles with a core of tightly packed plasmid DNA (pDNA) surrounded by a dense shell layer of PEG (Figure 1b). Because of the hydrophilicity as well as the strong steric–repulsive propensity of the PEG shell, the polyplex micelles are assumed to be stable in physiological entities including harsh *in vivo* conditions.[11] Furthermore, after internalization of the polyplex micelles into cellular compartments through the endocytic pathway, the ethylenediamine unit in the block copolymer is expected to facilitate efficient

Correspondence: Professor K Kataoka, Department of Materials Engineering, Graduate School of Engineering, The University of Tokyo, 7-3-1 Hongo, Bunkyo-ku, Tokyo 113-0033, Japan.
E-mail: kataoka@bmw.t.u-tokyo.ac.jp
Received 16 September 2006; revised 24 January 2007; accepted 31 January 2007; published online 26 April 2007

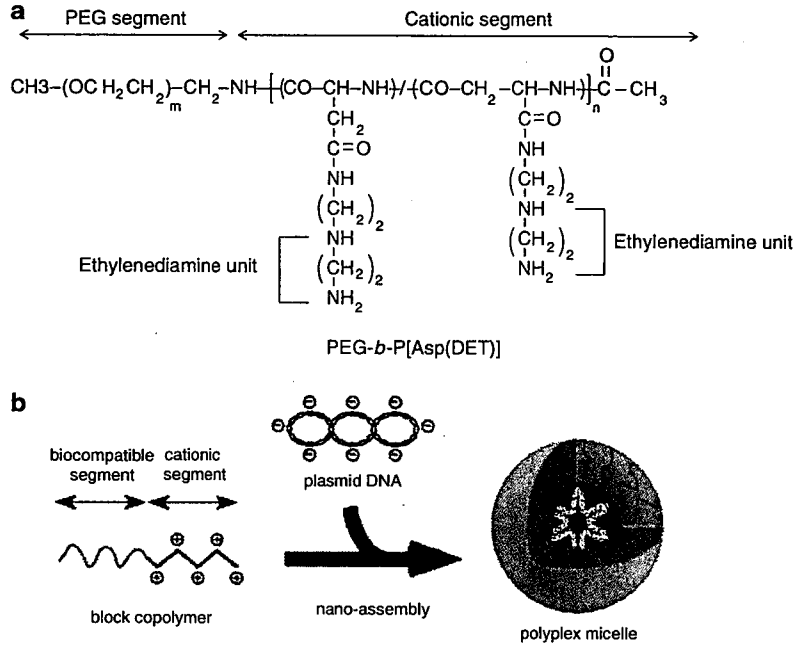

Figure 1 (a) Chemical structure of PEG-*b*-P[Asp(DET)] block copolymer. (b) Schematic illustrations of the polyplex micelle formation through electrostatic force.

translocation of the micelle toward the cytoplasm due to the proton sponge mechanism based on its high buffering capacity.[12] A previous study indeed revealed that polyplex micelles made from PEG-*b*-P[Asp(DET)] accomplished appreciably high gene transfection efficacy with remarkably low cytotoxicity toward several cultured cell lines as well as primary osteoblasts.[10]

In the present study, the utility of the polyplex micelle from PEG-*b*-P[Asp(DET)] for transfection to vascular lesions was investigated to evaluate its feasibility for vascular gene therapy. The polyplex micelle was revealed to have excellent colloidal stability even in proteinaceous medium and reduced interactions with blood components, showing appreciable gene transfection efficacy toward primary vascular smooth muscle cells (VSMC) under *in vitro* conditions. Furthermore, *in vivo* transfection of a reporter gene to rabbit carotid artery with induced neointimal lesions was successfully done, with high transfection ability and markedly reduced cytotoxicity and thrombogenicity of the polyplex micelles, making it feasible for vascular gene therapy.

Results

In vitro *gene transfer to VSMC*

The gene expression efficacy was evaluated as expressed luciferase activity. Expression pDNA containing the luciferase gene (*pCAccluc+*) was transferred to cultured VSMC using the polyplex micelle from PEG-*b*-P[Asp(DET)] to assess the gene transfection efficiency of the micelle from the activity of expressed luciferase after 48 h of culture. Polyplexes from branched polyethyleneimine (BPEI) and P[Asp(DET)] were used as controls. Note that P[Asp(DET)] is the homopolymer of Asp(DET), and was selected as a control to estimate the effect of PEG

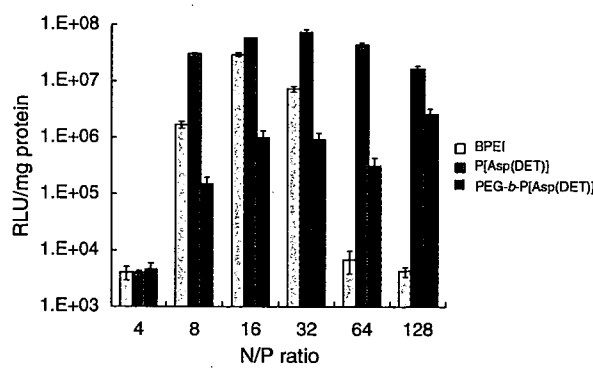

Figure 2 *In vitro* gene expression as measured by luciferase activity at 48 h after administration of BPEI polyplex, P[Asp(DET)] polyplex and PEG-*b*-P[Asp(DET)] micelle. Each polymer was complexed with pCAcc-luc+ at various N/P ratios, and applied to cultured VSMC. Forty-eight hours later, the cells were lysed, and luciferase activity of the lysates was measured. Values are expressed as RLU/mg protein. Values are shown as mean±s.e.m.

on physicochemical and biological characteristics of the polyplexes. Polyplexes of BPEI and P[Asp(DET)] as well as polyplex micelles of PEG-*b*-P[Asp(DET)] were prepared by mixing the corresponding polymer with pDNA at various N/P ratios. Here, N/P ratio refers to the unit molar ratio of the amino group in the polymer to the phosphate group in the pDNA. BPEI polyplex showed maximum transfection at an N/P ratio of 16 (Figure 2), followed by a steep decrease in efficacy, presumably due to increased cytotoxicity, as shown in Figure 3. Notably, VSMC transfected with P[Asp(DET)] polyplex and PEG-*b*-P[Asp(DET)] polyplex micelle maintained appreciably high luciferase activity at a wide range of N/P ratios >8, consistent with their lowered cytotoxicity (Figure 3). P[Asp(DET)] polyplex achieved more than tenfold higher

transfection activity than the PEG-*b*-P[Asp(DET)] micelle under this condition, and was even more effective than BPEI polyplex. It should be noted that transfection was not detectable for naked pDNA under the same conditions (data not shown).

Cytotoxicity to VSMC

Cytotoxicity to VSMC of the polyplexes and the polyplex micelles with varying N/P ratios was evaluated by MTT assay after 48 h of incubation. The viability of cells incubated with BPEI polyplex decreased linearly with an increase in N/P ratio, as seen in Figure 3. In contrast, cellular viability remained at more than 70 and 90% even after 48 h incubation with P[Asp(DET)] polyplex and PEG-*b*-P[Asp(DET)] polyplex micelle, respectively, up to an N/P ratio of 64.

Aggregate formation in albumin solution

To assess the colloidal stability of the polyplexes in biological media, they were subjected to measurements of particle size and ζ-potential after incubation for 1 h in phosphate-buffered saline (PBS) containing various concentrations of albumin. The polyplex micelle prepared at N/P = 40 maintained a size of approximately 110 nm regardless of albumin concentration, as summarized in Table 1, yet polyplexes from both BPEI (N/P = 10) and P[Asp(DET)] (N/P = 40) exhibited a marked increase in particle size in medium containing albumin at 1–2 mg/ml. The polyplexes from BPEI and P[Asp(DET)] showed highly positive ζ-potential values (~26 mV) in the absence of albumin, whereas their ζ-potential values decreased toward a neutral value with an increase in albumin concentration, presumably due to the association with anionically charged albumin molecules (Figure 4). This nonspecific association with albumin is likely to be the reason for the aggregate formation of the polyplex system in the presence of albumin observed in Table 1. In contrast, the polyplex micelle had an almost neutral ζ-potential with a small absolute value over a wide range of albumin concentrations (Figure 4), indicating improved colloidal stability of the polyplex micelle compared to conventional polyplexes with a cationic nature.

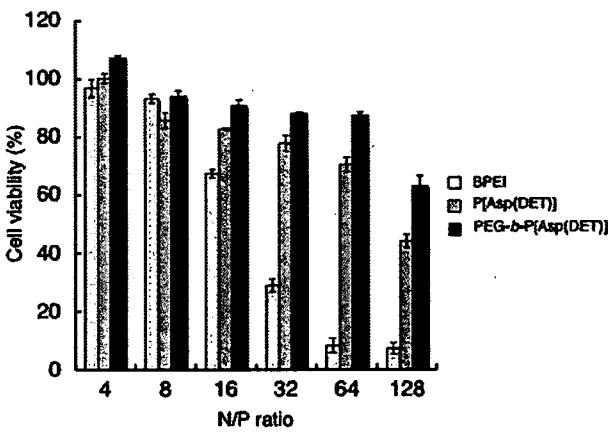

Figure 3 *In vitro* cytotoxicity to VSMC after 48 h incubation with BPEI polyplex, P[Asp(DET)] polyplex and PEG-*b*-P[Asp(DET)] micelle. Each polymer was complexed with pDNA at various N/P ratios, and applied to cultured VSMC ($n = 4$, each). Forty-eight hours later, cell viability was assessed by MTT assay. Values are shown as mean ± s.e.m.

Measurement of platelet aggregation using platelet-rich plasma

It is known that platelet aggregation plays a pivotal role in the initial stage of the thrombus formation. To estimate the thrombogenicity of the polyplexes and micelles, they were mixed with platelet-rich plasma (PRP), and the platelet aggregation was evaluated by a laser-scattering aggregometer PA-200 (Kowa, Tokyo, Japan). In this measurement, aggregate formation was measured as an increase in the light-scattering intensity (LSI; in mV). The size of detected aggregates was tentatively defined by LSI and was classified as 'small', 'medium' and 'large' as

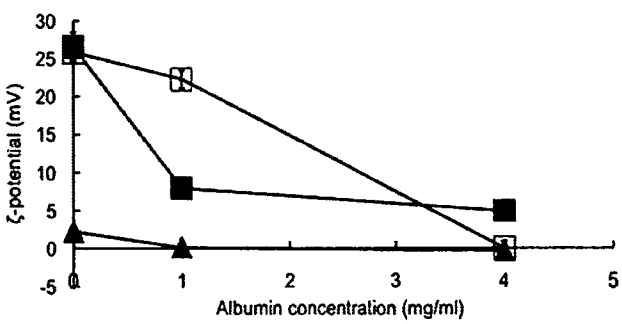

Figure 4 ζ-potential of BPEI polyplex (N/P = 10) (open squares), P[Asp(DET)] (N/P = 40) (solid squares), and PEG-*b*-P[Asp(DET)] micelle (N/P ratio = 40) (triangles) in the medium containing varying concentrations of albumin solution ($n = 3$). Values are shown as mean ± s.e.m.

Table 1 Particle size analysis in the medium with varying albumin concentrations (nm)

	Albumin concentration (mg/ml)					
	0	*0.01*	*0.1*	*1*	*2*	*4*
BPEI polyplex	136.3	130.0	131.3	141.7	ND[a]	ND[a]
P[Asp(DET)] polyplex	141.7	120.3	167.3	ND[a]	ND[a]	ND[a]
PEG-*b*-P[Asp(DET)] micelle	112.0	108.7	117.7	111.3	112.7	111.7

Abbreviations: BPEI, branched polyethyleneimine; ND, not determined; PEG, poly(ethylene glycol).
BPEI N/P = 10, P[Asp(DET)] N/P = 40, PEG-*b*-P[Asp(DET)] N/P = 40.
[a]Not determined because of aggregate formation.